INVESTIGATION OF ION TRANSPORT PROPERTIES OF ORGANIC ELECTROCHEMICAL TRANSISTORS

A Thesis Submitted to
the Graduate School of
İzmir Institute of Technology
in Partial Fulfillment of the Requirements for the Degree of

MASTER OF SCIENCE

in Chemistry

by
Tuğçe KÜÇÜKTARTAR

December 2022
İZMİR

ACKNOWLEDGEMENTS

It is a great pleasure for me to extend my gratitude to everyone who contributed in various ways throughout my master's education.

Firstly, I would like to thank my advisor Assoc. Prof. Dr. Ümit Hakan YILDIZ for given me the opportunity to be part of his group. I studied very motivated thanks to his teachings, inspiring ideas, encouragement and support.

I am very grateful to Prof. Dr. Cem ÇELEBİ and his group members for generously sharing their lab facilities and knowledges. Besides, I would like to acknowledge to Dr. Ayşegül ERDOĞAN and Dr. Meral ESEN, Ege University Central Research Testing and Analysis Laboratory Research and Application Center (EGE MATAL).

I would like thank my lovely lab mate Dilce ÖZKENDİR İNANÇ and all members of the BIOMACROS group for their friendship, accompany and help during my studies. It was my pleasure to work with all of you guys.

I also very thankful to my colleagues Suay DARTAR, Ezgi VURAL, Beraat Umur KAYA, Nehir NALINCI BARBAK and my dear friends Deniz SALUCU, Sibel ATİLA, Öykü KOCAMAN for their endless support in all matters.

Special thanks to Yankı Öncü YAYAK, who has always supported and encouraged me, made my life easier and cheered.

Last but not least, I can't thank my family enough for always being there for me with incredible devotion under all circumstances. I owe you my career, I dedicate this thesis to you and love you very much.

ABSTRACT

INVESTIGATION OF ION TRANSPORT PROPERTIES OF ORGANIC ELECTROCHEMICAL TRANSISTORS

Organic electrochemical transistors (OECTs) comprise large amplification in current response while operating at low voltages and have high transconductance due to its volumetric capacitance created by ion injection from electrolyte through the whole organic semiconductor channel. OECTs are switchable by doping and de-doping of active channel via application of positive or negative gate bias. One of the most common organic material for OECTs is the conductive polymer, poly(3,4-ethylenedioxythiophene) polystyrene sulfonate (PEDOT:PSS). PEDOT:PSS offers prominent advances because of their coupled electronic and ionic conductance, morphology and optical properties. Although the complex working principle of OECT has been tried to be elaborated with several models in literature, the conduction of ions and electrons in the channel has not been fully elucidated. In this thesis, the transformations between un-doped, doped and de-doped state investigated systematically based on the electrical (OECT), structural and morphological characterization of PEDOT:PSS thin film. Measurements were conducted with different dopant molecules and the repeatability of the device was investigated. As a result, the most stable drain and gate voltage range in which the device works has been determined. In addition, the X-ray photoelectron spectroscopy (XPS) investigation performed which is revealed that the density of the bipolaron formation of PEDOT:PSS in the doped state increase as compared to its natural form in the de-doped state. XPS mapping on OECT devices suggested that ions migration is homogeneously generated by applied bias.

ÖZET

ORGANİK ELEKTROKİMYASAL TRANSİSTÖRLERİN İYON TAŞINMA ÖZELLİKLERİNİN İNCELENMESİ

Organik elektrokimyasal transistörler (OECT'ler), düşük voltajlarda çalışırken akım tepkisinde büyük amplifikasyon yaratırlar ve tüm organik yarı iletken kanal boyunca elektrolitten iyon enjeksiyonu ile oluşan hacimsel kapasitansı nedeniyle yüksek iletkenliğe sahiptirler. OECT'ler, pozitif veya negatif kapı gerilimi uygulanarak aktif kanalın katkılı (dope) veya katkısız (de-dope) hale getirilmesi ile değiştirilebilir. OECT'ler için en yaygın organik malzemelerden biri iletken polimer, poli(3,4-etilendioksitiyofen) polistiren sülfonattır (PEDOT:PSS). PEDOT:PSS, birleşik elektronik ve iyonik iletkenlikleri, morfolojileri ve optik özellikleri nedeniyle önemli avantajlar sunar. OECT'nin karmaşık çalışma prensibi literatürde çeşitli modellerle ifade edilmeye çalışılmışsa da iyonların ve elektronların kanaldaki iletimi tam olarak aydınlatılamamıştır. Bu tezde, PEDOT:PSS ince filminin elektriksel (OECT), yapısal ve morfolojik karakterizasyonuna dayalı olarak başlangıç (un-dope), katkılı (dope) ve katkısız (de-dope) durum arasındaki dönüşümler sistematik olarak incelenmiştir. Farklı dopant molekülleri ile ölçümler yapılmış ve cihazın tekrarlanabilirliği araştırılmıştır. Sonuç olarak cihazın çalıştığı en kararlı drenaj ve kapı voltaj aralığı belirlenmiştir. Ek olarak, gerçekleştirilen X-ışını fotoelektron spektroskopisi (XPS) araştırması, PEDOT:PSS'nin katkılı durumdaki bipolaron oluşumunun yoğunluğunun, katkısız durumdaki doğal formuna kıyasla arttığını ortaya koymaktadır. OECT cihazlarındaki XPS haritalaması, iyon göçünün uygulanan voltaj tarafından homojen bir şekilde üretildiğini öne sürmüştür.

TABLE OF CONTENTS

LIST OF FIGURES

Figure **Page**

Figure **Page**

Figure **Page**

LIST OF TABLES

CHAPTER 1

INTRODUCTION

1.1. Conducting Polymers

In the last few decades, conducting polymers (CP) have attracted attention with their wide applications and continuously improved properties; in a simplest definition, conducting polymers are type of organic (semi)conductors which have conjugated structures that contain alternating double and single bonds in their backbone. This conjugation allows the electrons to flow through the polymer chain. However, the conductivity of these polymers are quite low. According to the Shirakawa, MacDiarmid and Heeger's work in 1977 on trans-polyacetylene and its conductivity which later won the Nobel Prize in 2000, the electrical conductivity of polyacetylene exposed to halogen vapors was increased ten million times. In that case polymer chains were doped with halogens, which reduces the band gap and increases the carrier density to achieve a conductive level.[1] The expression of semiconductors compared to conductors and insulators can be done more easily with band theory (Figure 1.1). The increase in the number of monomers in the conjugate chain causes a raise in the overlapping of atomic orbitals to form molecular orbitals, resulting in two types of bands: valence band (bonding orbitals overlap), conduction band (overlapping antibonding orbitals). The gap formed by the energy difference between highest occupied molecular orbital (HOMO) and lowest unoccupied molecular orbital (LUMO) is defined as the band gap (Eg). If the band gap is too large, the electrons cannot jump to the conduction band and the material is called as insulator. If there is no gap between the valence band and the conduction band, the electrons move freely and pass to the conduction band, and in this case the material is called conductor. For semiconductors, band gap is small enough to excitation of an electron to conduction band when leaving behind a positive hole.[2]

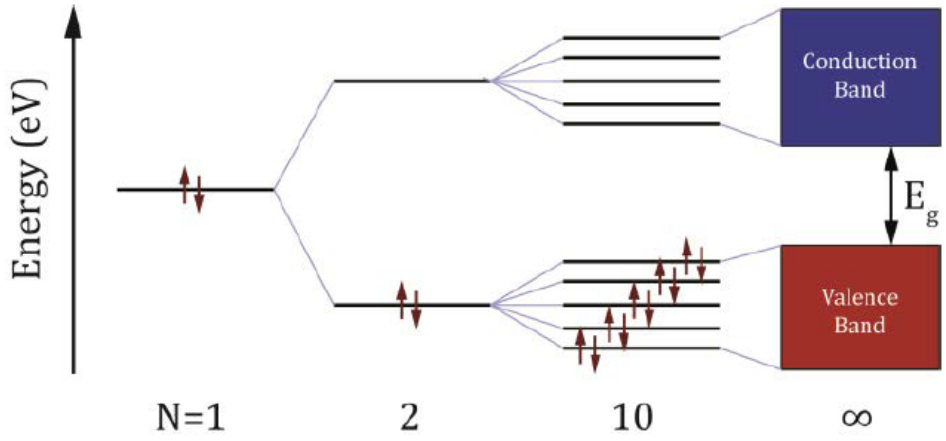

Figure 1.1. Valence and conduction bands of conjugated polymers. "N" refers number of units that interact.[2]

The conductivity of organic semiconductors can be enhanced via oxidation or reduction process (in solid-state physics, called p-type and n-type doping, respectively) which increase charge carrier mobility. Briefly, p-type doping means removing an electron from the valence band (HOMO), and n-type doping refers contribution of electron to the conduction band (LUMO) (Figure 1.2). In p-type doping, electron affinity (EA) of dopant molecules has higher or equal to the ionization energy (IE) of CP matrix. However, for n-type doping, dopants have lower IE than CP matrix.[3]

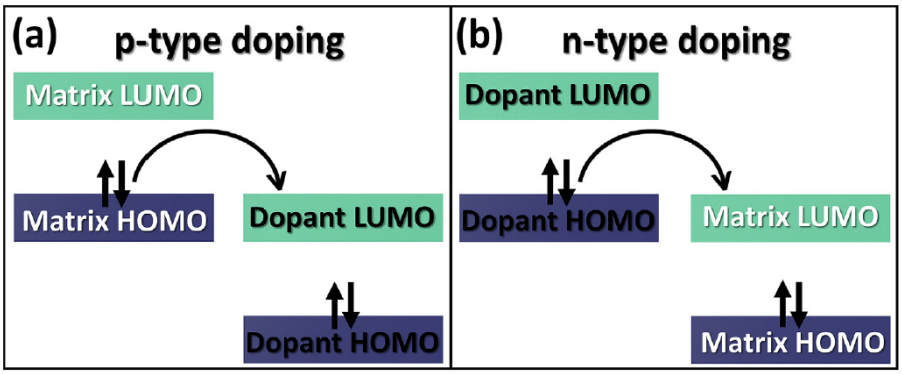

Figure 1.2. Schematic representation of p-type (a) and n-type (b) doping.[4]

1.1.1. PEDOT:PSS

Poly(3,4-ethylenedioxythiophene)-poly(styrenesulfonate) (PEDOT:PSS) is a typical conducting polymer used in organic electronics. It consists of holes on the positively charged PEDOT chains interacted with sulfonate ions in the PSS chains.[5] PEDOT:PSS has a property of a mixed electronic-ionic conductor due to its structure.[6] Besides, it has excellent features such as good film-forming ability with facile fabrication techniques, optical transparency in the visible light range, and good physical and chemical stability in air. It offers prominent advances in applications involve bioelectronics, flexible electronics, optoelectronics and energy storage devices because of their combined electronic and ionic conductance, morphology and optical feature.[7,8]

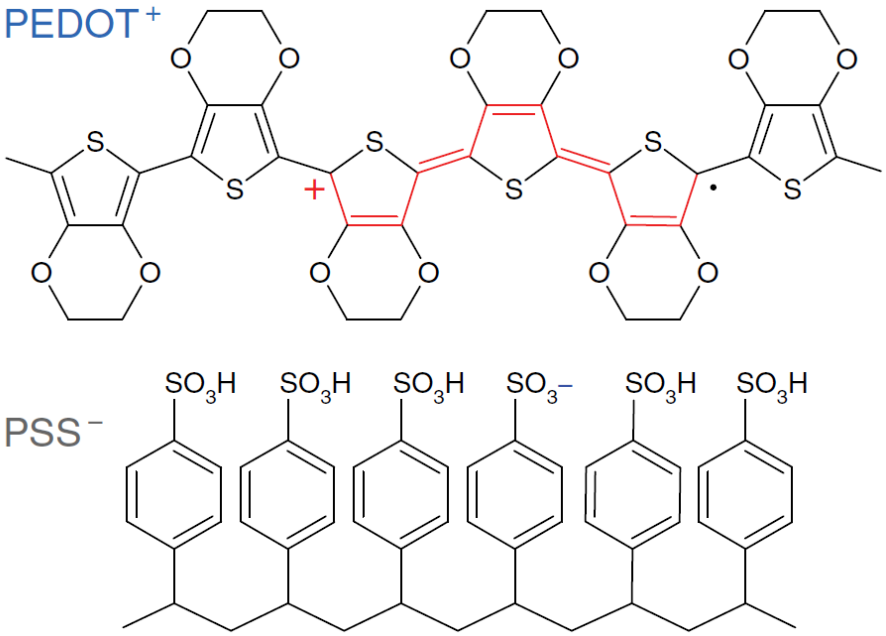

Figure 1.3. Chemical structures of PEDOT:PSS[6]

Although facile fabrication methods, pristine PEDOT:PSS film is not durable in aqueous environment. To improve its stability organosilane based compounds used for crosslinking PEDOT:PSS film to prevent its dissolution and delamination. The most common one is (3-glycidyloxypropyl)trimethoxysilane (GOPS).[9,10,11] On the other hand, one of the studies shows that divinylsulfone is also used to crosslink of PEDOT:PSS.[12]

To improve fabrication and conductivity of PEDOT:PSS films there are numerous

studies in current literature. The most common ones are secondary doping[13] by treatment with organic solvents[14,15,16,17] (e.g., ethylene glycol (EG), dimethyl sulfoxide (DMSO), dimethylformamide (DMF), tetrahydrofuran (THF) etc.), ionic liquids[18], surfactants[19,20] (e.g., sodium dodecyl sulfate (SDS), hexadecyltrimethylammonium bromide (CTAB)) or acids (e.g. H_2SO_4, H_2PO_4)[21,22,23].

1.2. Organic Electrochemical Transistors

Organic electrochemical transistors (OECTs) consist of thin organic semiconductor film contact with source and drain electrodes and an electrolyte between gate and semiconductor channel. It differs from the most widely preferred organic field-effect transistors (OFETs) in organic electronics by having electrolyte instead of dielectric in contact with semiconductor channel (Figure 1.4).[24]

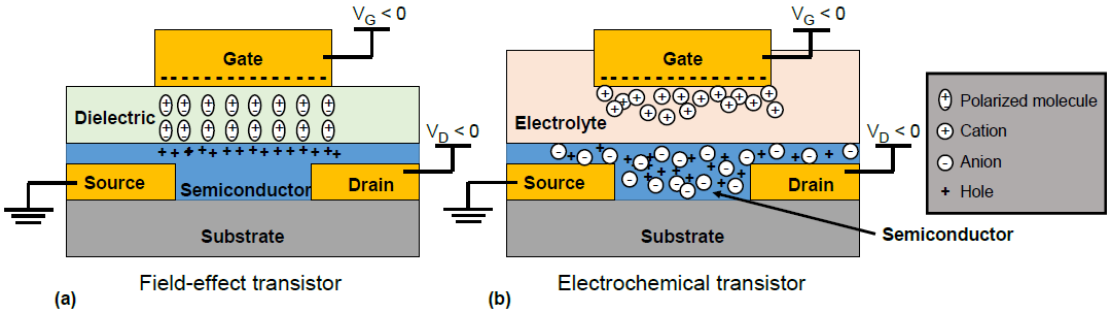

Figure 1.4. Illustration of an OFET (a) and OECT (b) structure. In the OFET, the applied gate bias polarizes the dielectric and charge transfer occurs at the interface between dielectric and semiconductor. In the OECT, charge transfer occurs throughout the volume of device when ions injected from electrolyte into the semiconductor channel under applied gate bias.[24]

In 1984, it is discovered that the reversible modulation of conductivity could be achieved by changing the redox (doping) state of organic semiconductor film by applying bias with gate electrode.[25] In addition, the output signal can be amplified, and the device can be switched with an application of gate bias. Unlike OFETs, with the use of electrolytes in OECTs, not only the doping state of the channel interface, but also the doping state of the entire volume is changed. This characteristics of OECT provides high amplification

in the output current at low voltages.[26] Thanks to the unique features of OECTs, they are compatible for biosensing in aqueous media. Furthermore, there are numerous applications of OECTs have been studied such as chemical and biosensing,[27,28], enzyme[29,30,31,32,33,34] and metabolite sensing[35], neural activity detection[36,37,38,39], integrated circuits.[40,41,42]

1.2.1. OECT Working Principle

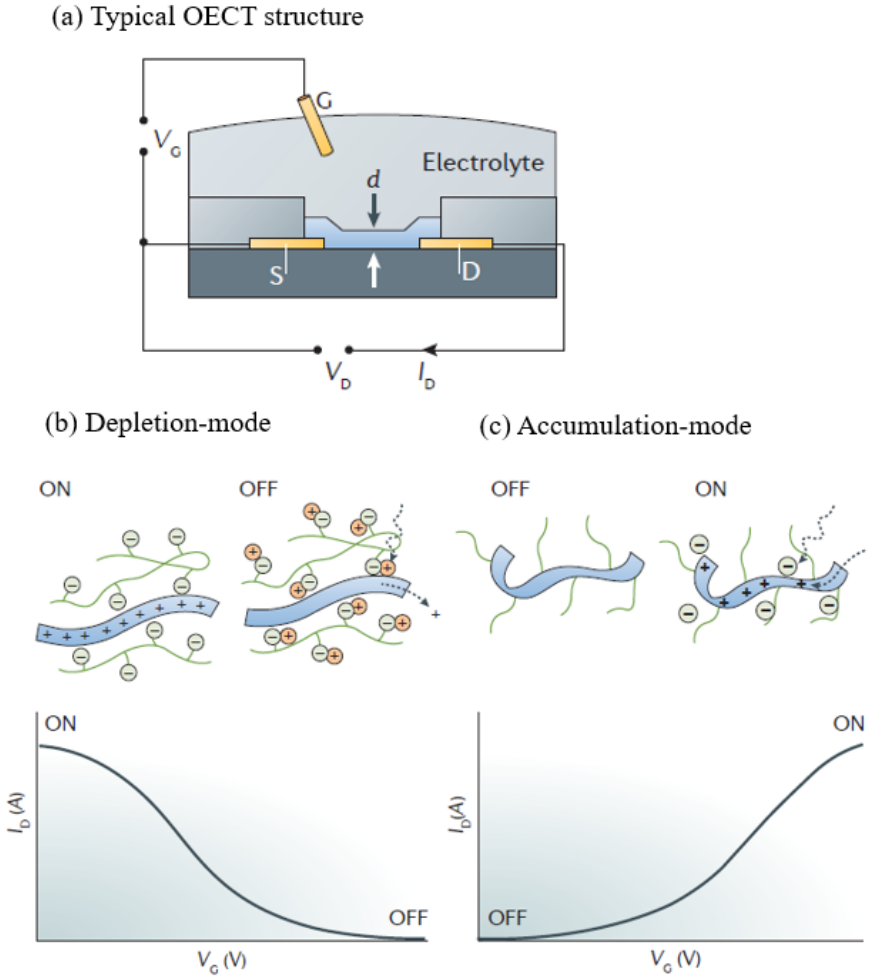

Figure 1.5. Typical structure (a) and operation mode of OECT and typical transfer curves of drain current versus gate voltage for depletion and accumulation-mode, respectively (b, c).[26]

A schematic of a typical OECT set-up is shown in Figure 1.5a. The operation modes of OECTs depends on the characteristics of the organic semiconductor channel (doping

state). In depletion-mode transistors, the semiconductor is naturally in its conductive state. A p-type PEDOT:PSS is an example of depletion-mode OECTs. Positive holes (h^+) formed on the PEDOT chain with the electron withdrawal of PSSs creates positively charge carriers and enable PEDOT:PSS to p-type semiconductor. In depletion-mode transistors, the semiconductor is naturally in its conductive state (Figure 1.5b). When a positive bias applied to the gate electrode, cations (X^+) injected into a semiconductor channel and sulfonate ions of PSS are compensated. The drop in current flow occurs as a result of the decrease in charge carries (holes) on PEDOT backbone and $PEDOT^+$ is reduced its non-conductive (neutral) state. When gate bias turn back to zero volt, the cations diffuse back to the electrolyte and new ionic bonds build between sulfonate ions in PSS and PEDOT chains. This reversible process is shown in the equation 1.1.[24]

$$PEDOT^+ : PSS^- + X^+ \rightleftharpoons PEDOT^0 + X^+ : PSS^- + h^+ \tag{1.1}$$

In accumulation-mode transistors, the semiconductor is neutrally in its non-conductive state with a small amount of holes (Figure 1.5c). Conductivity of the semiconductor is promoted by an application of negative gate bias. When negative gate bias applied, anions injected into the channel, holes are accumulated and channel is doped.[26,43]

1.2.2. Device Models

In the previous section, it is emphasized that a large drain current amplification can be achieved by an application of low gate voltage. The transduction process is expressed with a transfer curve by plotting the drain currents (I_{ds}) versus gate voltages (V_{gs}) (Figure 1.5b,c) and the efficiency in transduction can be determined by calculating first derivative of the transfer curve (equation 1.2). Thus, the result which named as transconductance (g_m) is proportional to the amplitude of the output signal.

$$g_m = \frac{\partial I_D}{\partial V_G} \tag{1.2}$$

For optimization of device design, the output behavior of OECTs has been tried to be explained with many models in the literature. The two standard model, which are still the most frequently used for expressing basic OECT behavior, were introduced by Bernard and Malliaras in 2007. These models define the steady state and transient behaviours

of OECTs. The main difference of these models is that transient conditions include the diffusion of ions where the ionic gate current is not zero however, it is assumed to be zero at steady state conditions.[44]

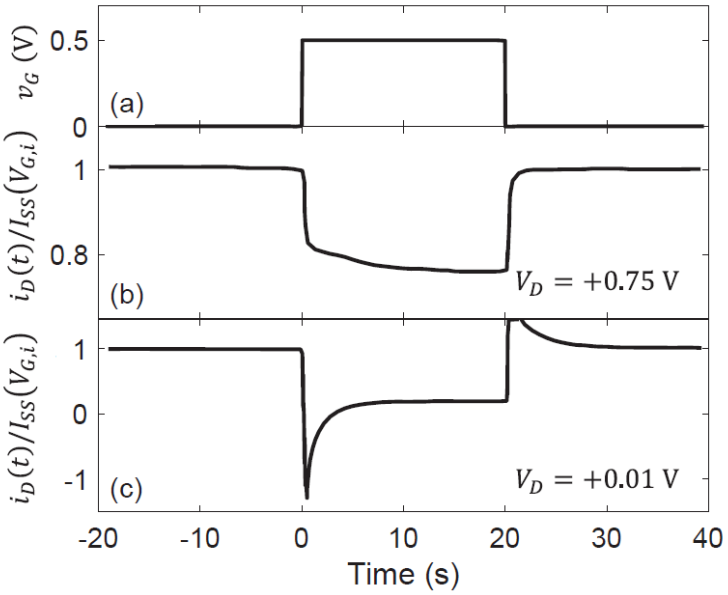

Figure 1.6. The normalized drain-source current responses plotted for various drain voltages (0.75 V and 0.01 V) under the application of square step gate voltage.[44]

In Figure 1.6, the transient behaviour is shown by measuring the drain-source current under application of square step gate voltage. Figure 1.6b shows that electronic transfer is faster than ionic charge transfer since the more steady relaxation is observed in drain current however in Figure 1.6c, when ionic charge transfer is faster than electronic transfer, the drain current first drop sharply then returns its initial state exponentially.

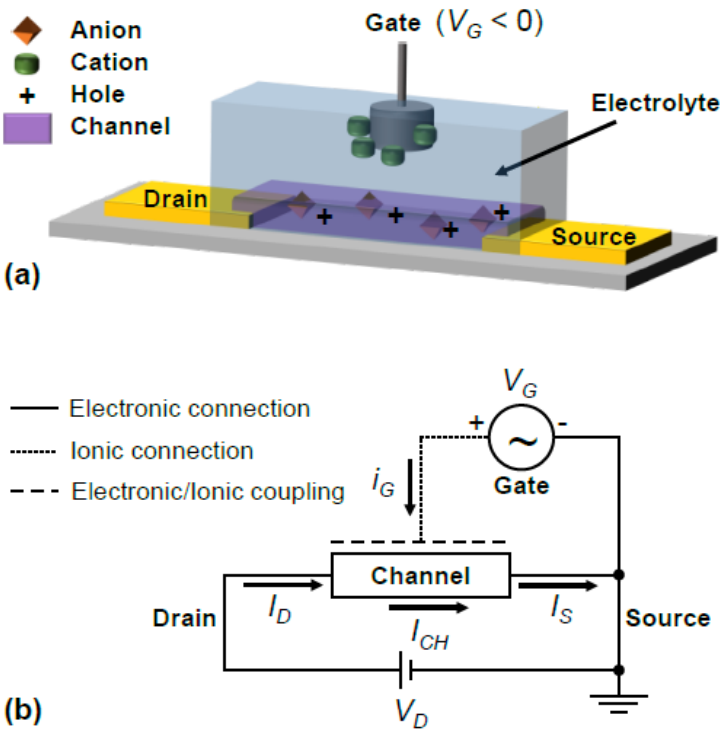

Figure 1.7. Standard structure (a) and circuit diagram (b) of an OECT (i_G: the ionic gate (transient) current, I_{CH}: the channel current, I_D: the drain current, I_S: the source current, V_D: the drain voltage, and V_G: the gate voltage

According to these models, the device physics depends on the combination of ionic and electronic charge carriers and assumptions were made for depletion-mode transistor with a p-type semiconductor. The device circuit consist of two circuits: ionic and electronic circuit are shown in Figure 1.7[45,46] Ionic circuit includes ionic charge transport in between the gate-electrolyte-channel and electronic circuit comprise of electron transfer including hole density and transport between the source-channel-drain.

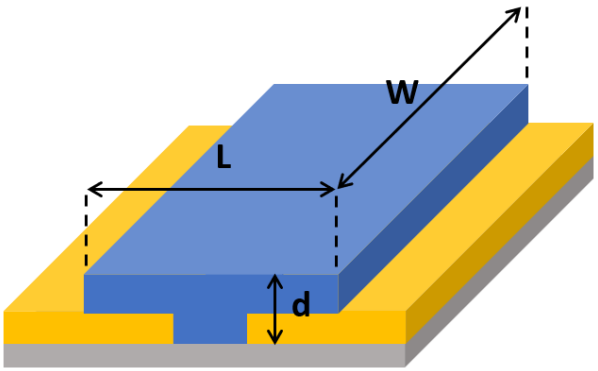

Figure 1.8. The illustration of channel geometry of an OECT.

In addition to this approximation, the effect of device geometry to the transconductance is also investigated. As a result of many studies, it has been revealed that in a system with mixed/ionic electronic conduction, the transconductance value depends on the film thickness(d) and channel geometry(W: channel width, L: channel length) as well as the μC^* product (μ: hole mobility, C^*: volumetric capacitance), which is an important figure of merit for OECTs as shown in the equation1.3. μC^* is depends on the property of semiconductor material and both can be determined by experimentally.[43,47,48,49,50] The resulting sign of the expression is determined by considering the magnitude of threshold voltage V_T. The device geometry is illustrated in Figure 1.8.

$$g_m = \begin{cases} -\mu C^* \frac{Wd}{L} V_D, & \text{for } V_D > V_G - V_T \\ \mu C^* \frac{Wd}{L} [V_G - V_T], & \text{for } V_D < V_G - V_T \end{cases} \tag{1.3}$$

On the other hand, the other considerations such as parasitic contact resistance[48,51] that contributes the total device resistance, the effect characteristics of channel material,[45] the choice of gate material and electrolyte still discussed for device design and optimizations.[46]

CHAPTER 2

EXPERIMENTAL

2.1. Materials

Poly(3,4-ethylenedioxythiophene)-poly(styrenesulfonate) (PEDOT:PSS) 1.3 wt % dispersion in H2O, conductive grade, (3-Glycidyloxypropyl) trimethoxysilane $\geq 98\%$ (GOPS) were purchased from Sigma Aldrich. Ammonium hyroxide solution (28-30 % NH_3 basis, Merck), hydrogen peroxide (30 %, Sigma Aldrich) and Mili-Q water (R=18.2 MΩ) were used for substrate (RCA) cleaning. 3 mm Poly(methyl methacrylate) (PMMA) sheets were used as the electrolyte cell, and double-sided tape (3m) was used to fix the sheets to the surface. Potassium chloride (Merck), Potassium peroxymonosulfate (OXONE, Sigma Aldrich), N,N-Bis(2-hydroxyethyl)-2-aminoethanesulfonic acid (BES) sodium salt (Sigma Aldrich), N-Methyldiethanolamine (MDEA, Sigma Aldrich) were used for the preparation of electrolytes.

2.2. Device Fabrication

The fabrication of the OECT device used in this study consists of three parts described in the following sections. First, the gold-glass electrodes were prepared. Next, they were functionalized with the chemicals mentioned in the materials part and finally, PMMA cells for electrolytes were placed on the gold electrode surfaces with adhesive tape and made ready for OECT measurements (Figure 2.4).

2.2.1. Preparation of Gold Electrodes

As the first step, the microscope glass slides were cut in the form of 1x1 cm by diamond tip cutter, cleaned with RCA solution (NH_4OH : H_2O_2 : Mili-Q water, 1:1:5 v/v)

at 80 °C for 45 minutes, washed with plenty of water and dried with nitrogen. Pre-cleaned glass surfaces were treated with oxygen plasma (40 watt, 0.5 L/h gas flow) for 15 minutes to remove residual contamination. Next, the deposition of 4 nm chrome and 80 nm gold on the glass substrates was performed by thermal evaporation method in vacuum, respectively. Gold electrodes were deposited using masks with a gap of 150 μm. Thermal evaporation set up in quantum device laboratory was shown in Figure 2.1.

Figure 2.1. The Thermal Evaporation Set-up (a). The digital image of high vacuum system (b) consists of heater (1), monitor made of quartz crystal (2), sample holder (3), deposition materials (Cr (bottom left), Au (bottom right)[52]

2.2.2. Surface Functionalization

Prior to functionalization , the glass-gold electrode surface first cleaned and activated by RCA treatment as stated in the previous section. To obtain more stable polymer films anoxides layers are preferred due to its potential (mechanical and chemical stability,

heat transfer and conductivity) for functionalization of substrates by its high reactivity.[53] As previously introduced in section 1.1.1, PEDOT:PSS is not suitable for applications in aqueous media, GOPS is used to reduce the rate of swelling and delamination through increasing the crosslink density of the film however raise in the amount of GOPS cause decrease in the conductivity of the film.[54,55,56] In addition, organosilanes can quickly form covalent bonds with the substrate due to their better leaving groups. Thus, they are highly preferred in forming monolayers with oxide surfaces.[53]

In the study of Håkansson et al., the mechanism of GOPS crosslinking of PEDOT:PSS was investigated by photoelectron spectroscopy and interactions between GOPS-PEDOT:PSS and GOPS-substrate surface were proposed with an illustration in Figure 2.2. Figure 2.2a demonstrates the sulfonate groups of PSS bonded with epoxy ring of GOPS and covalent bond between three GOPS molecules. Figure 2.2b indicates the covalent bond between methoxysilanes of GOPS and hydroxyl groups of the glass surface.[56]

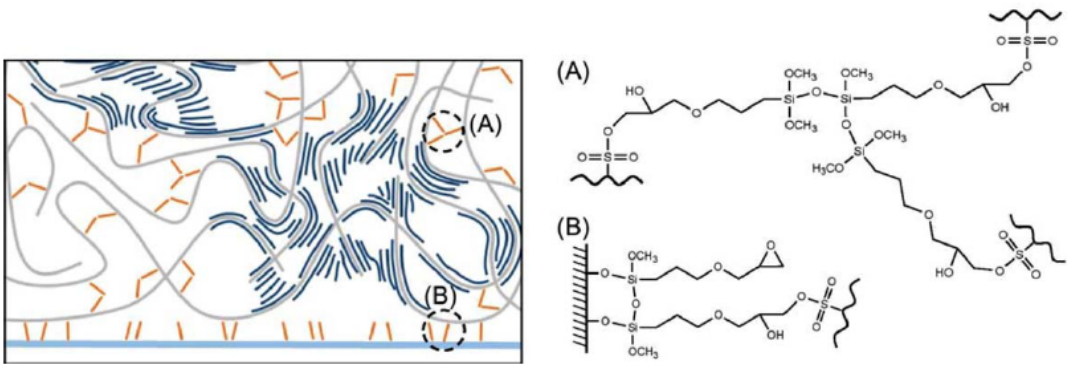

Figure 2.2. Illustration of GOPS interaction with PEDOT:PSS and substrate (glass) surface. (A) shows the interactions of PSS (grey)-GOPS (yellow) and GOPS-GOPS, (B) shows the interaction between GOPS and glass substrate surface.[56]

Despite the advance in fabrication of PEDOT:PSS, it has been suggested that the increase in the amount of GOPS reduces the conductivity of the film (Figure2.3).[56,57] Besides, one of the studies shows that GOPS crosslinking also causes undesired de-doping.[58]

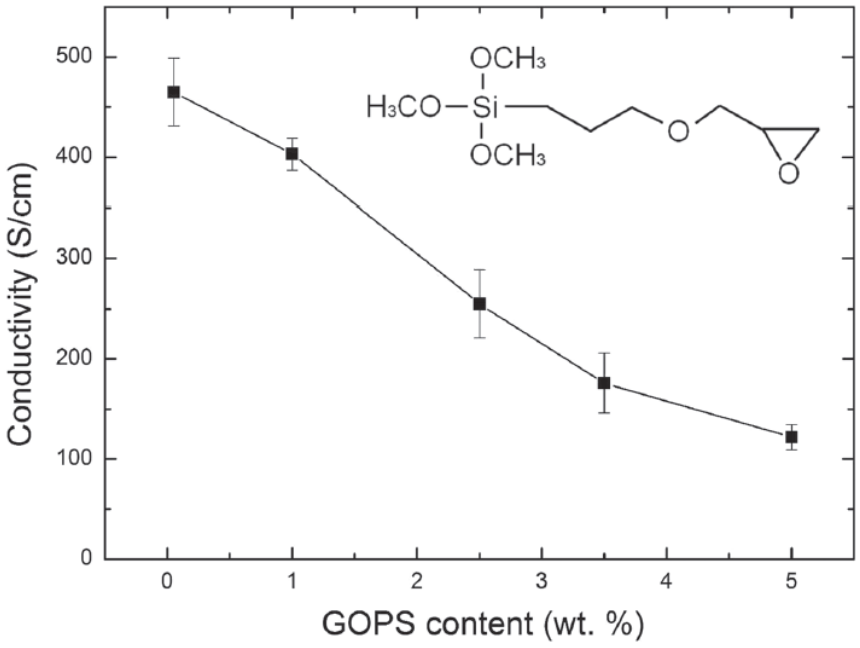

Figure 2.3. Conductivity of PEDOT:PSS films versus GOPS content of 0.05, 1, 2.5, 3.5, and 5. The chemical structure of GOPS shown upright of the graph.[57]

Considering the above-mentioned findings in section 1.1.1 and 2.2.2, the procedure was continued by incubating the activated surfaces in 1% v/v GOPS solutions for 3 hours. After that, the surfaces washed with Mili-Q water vigorously and dried with N_2. Next, 35 μL of 1.3% wt PEDOT:PSS aqueous dispersion was dropped only on the center of the surface and left to dry in ambient conditions. As a final step, they were washed with Mili-Q water until excess PEDOT:PSS removed then dried with N_2 (Figure 2.4).

2.2.3. PMMA-Cell Preparation

The electrolyte cells illustrated in the last step in the Figure 2.4 were cut from 3 mm PMMA sheets by Epilog Zing laser engraver. Vector cutting parameters were kept as 40 % speed, 70 % power. The cell geometry was created via CorelDRAW software.

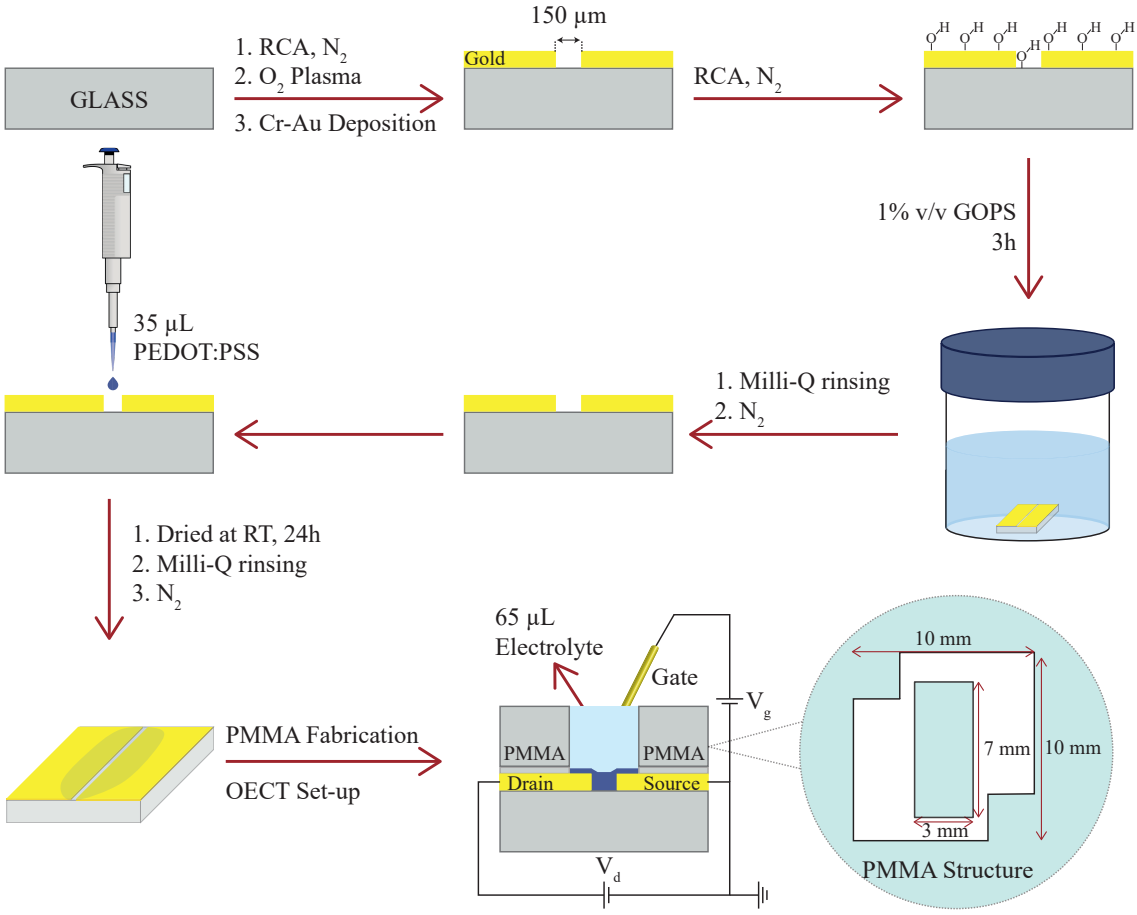

Figure 2.4. Schematic representation of experimental procedure for OECT fabrication and set-up

2.3. Characterization Techniques

The characterization methods used in overall study described in this section. The current-bias measurements were carried out to characterize the electrical properties of the film. The structural characterization of un-doped (neutral state of PEDOT:PSS), doped and de-doped state of surfaces performed by X-Ray Photoelectron Spectroscopy. In addition, topography information of the surface was obtained via Atomic Force Microscopy.

2.3.1. Electrical Characterization

For the OECT characterization, current-voltage measurements were performed by recording drain currents (I_{ds}) while sweeping the drain voltage (V_{ds}) 0 to 1 V with 0.05 V steps and keeping the gate voltage (V_{gs}) constant. I_{ds}-V_{ds} measurements were controlled by HP4145B semiconductor parameter analyzer with customized LabVIEW interface. The application of positive (0 to 1 V) and negative (0 to -1 V) gate bias were applied manually by 0.1 V intervals with HP34401 (digital multimeter). Initially, negative gate voltages were applied when the drain voltage sweeps and the output data recorded for each step. The measurements were followed by the application of positive gate voltage. The electrolyte volume kept constant as 65 μL during the measurements. Between the series of measurements, the surfaces were washed with Milli-Q water. Next, devices were dried with nitrogen to reduce swelling of PEDOT:PSS.[59,60] All measurements were carried out on a stable probe station consist of gold coated drain, source and gate probes (Figure 2.5).

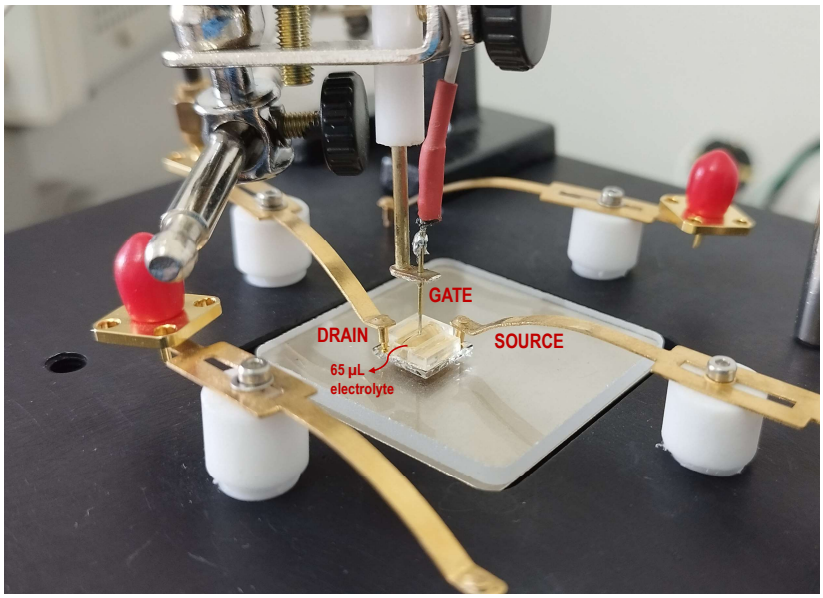

Figure 2.5. The photograph of OECT device with 65 μL electrolyte and probe station consist of drain, source and gate contacts

2.3.2. Spectroscopic Characterization

2.3.2.1. X-Ray Photoelectron Spectroscopy

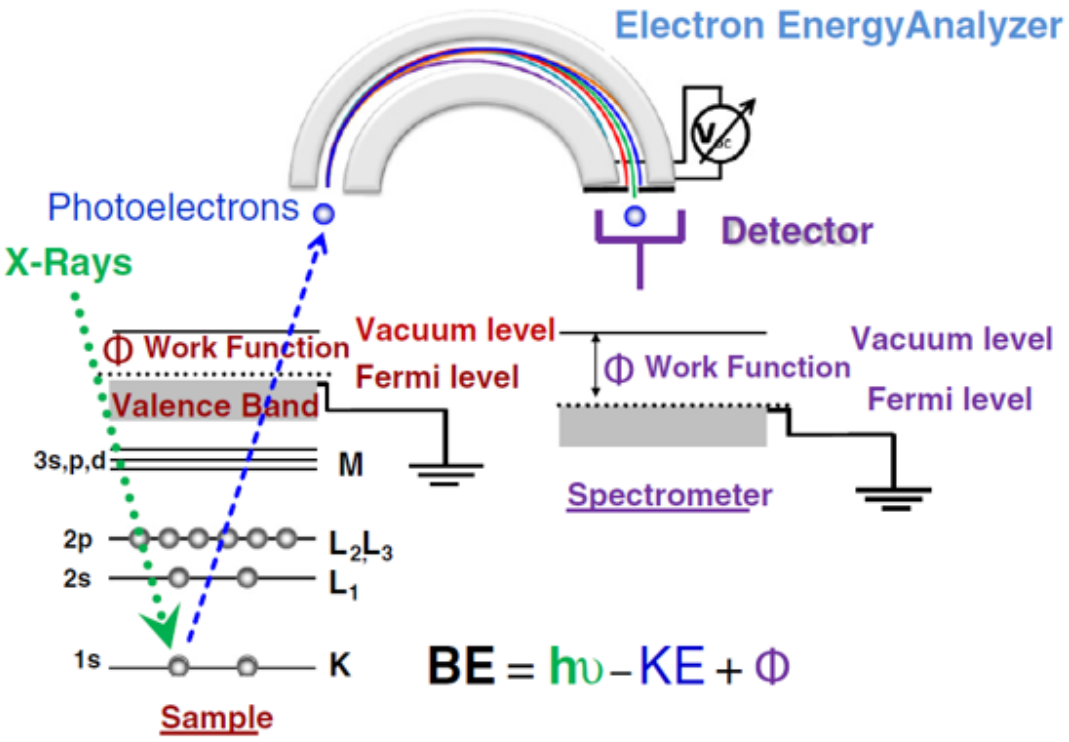

Figure 2.6. Schematic illustration of the X-Ray Photoelectron Spectroscopy[61]

X-ray photoelectron spectroscopy (XPS) is a powerful technique for characterization of the composition of a substrate surface. The principle of XPS technique based on photoelectric effect in which X-ray used as a photon source (Aluminum Kα or magnesium Kβ). In this technique, elemental information of surface is obtained by recording the kinetic energy resulted by emitted electrons and it provides binding energy value via expression in figure 2.6 (where BE refers to binding energy, KE is the kinetic energy of photoemitted electron, hν is the X-ray photon energy and ϕ is the work-function) that comes from the energy conservation of the photoelectric effect (Figure 2.6). In addition to the elementary characterization, atomic orbital types and oxidation states of species are

also be determined by using the binding energy values and peak shifts.[62,63] Furthermore, XPS analysis is performed in ultra-high vacuum condition since it is highly sensitive to the contamination of the surface.

2.3.3. Microscopic Characterization

2.3.3.1. Atomic Force Microscopy

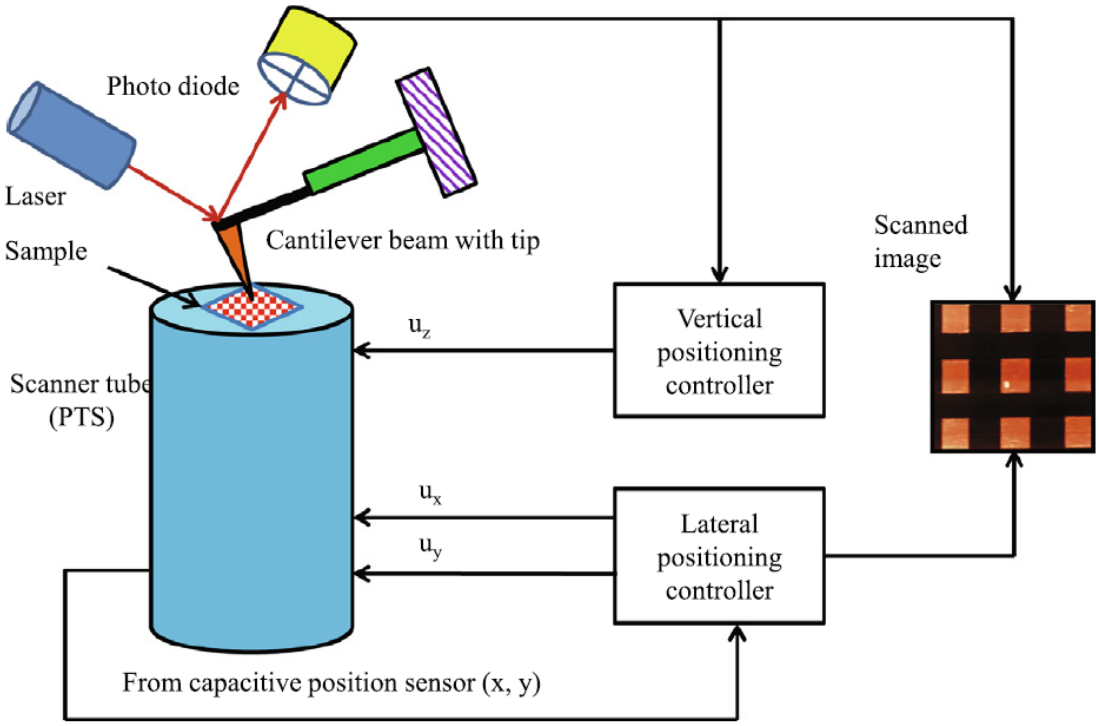

Figure 2.7. Schematic diagram of AFM components[64]

Atomic force microscopy (AFM) is a unique characterization technique that offers high resolution topography images and information about electrical and mechanical properties of various type of surfaces. AFM is useful method to characterize the surfaces since it provides details about the characteristics of surface at the nanometric scale.[65,66,67] Figure 2.7 shows the component of AFM including laser source, piezotube scanner, photodetector,

cantilever, position controller etc.[64]. Briefly, AFM is operated via two modes which are static and dynamic mode. In static mode, the cantilever tip has the constant contact with the surface. During scanning the surface, the displacement of the cantilever is detected via quantification of reflection of laser beam back of the cantilever and the surface profile information recorded by a photodetector. In dynamic mode, surface profile is recorded by measuring the change in oscillation amplitude and resonance frequency of cantilever tip. These parameters are related with interaction forces resulted between the cantilever tip and sample surface.[68,69]

CHAPTER 3

RESULTS & DISCUSSION

As mentioned in the Section 1.2, our OECT device belongs to the class of p-type, depletion-mode transistor, which is conductive in nature, non-conductive or less conductive when positive gate bias is applied, and its conductivity can be increased by manipulation with negative gate bias. When potassium chloride used as an electrolyte, under the positive gate bias, an electric field is created and thus potassium ions are pushed into the semiconductor channel and bind ionically with the PSS^{-}. The positive holes on the PEDOT chain are reduced and removed from the channel so that the channel is in the de-dope (insulating) state. When the magnitude of the gate voltage is zero or less than zero volts, diffusion of potassium ions takes place backwards through the channel and new PEDOT:PSS ionic bonds are formed.

Figure 3.1a, shows the response of the device under the gate bias applied from 0 to -1V, the current which passing through drain-source (I_{ds}) increases at least by a factor of two proportionally with the V_{ds} magnitude. Figure 3.1b shows the current value can be reduced at least ten times by application of gate bias from 0 to +1 V. It indicates that the active channel in OECT was successfully dope and de-doped by manipulation of the gate bias. Figure 3.1b also revealed that the I_{ds} values were not linearly increase while the drain voltage sweeps from 0.4 to 1V. Keeping the drain voltage larger than 0.4 V made de-doping of active channel more difficult as compared to low drain voltage (0 to 0.3 V_{gs}) in other words there is a current raise appears at this V_{ds} range. On the other hand, in Figure 3.1a, there is an amplification of the current response at drain voltage of 0.65 V. Despite this positive trend, this response may be generated by Faradaic processes, which also include electrolysis of the electrolyte solution.[44,60,70,71,72] Additionally, in Figure 3.1c, the I_{ds} responses versus V_{gs} are also demonstrated on the transfer curves by selecting three drain voltages as 0.2, 0.6 and 1 V. Typical depletion-mode behavior can be observed for all selected V_{ds} which the I_{ds} value decreases as the V_{gs} increases from negative to positive.

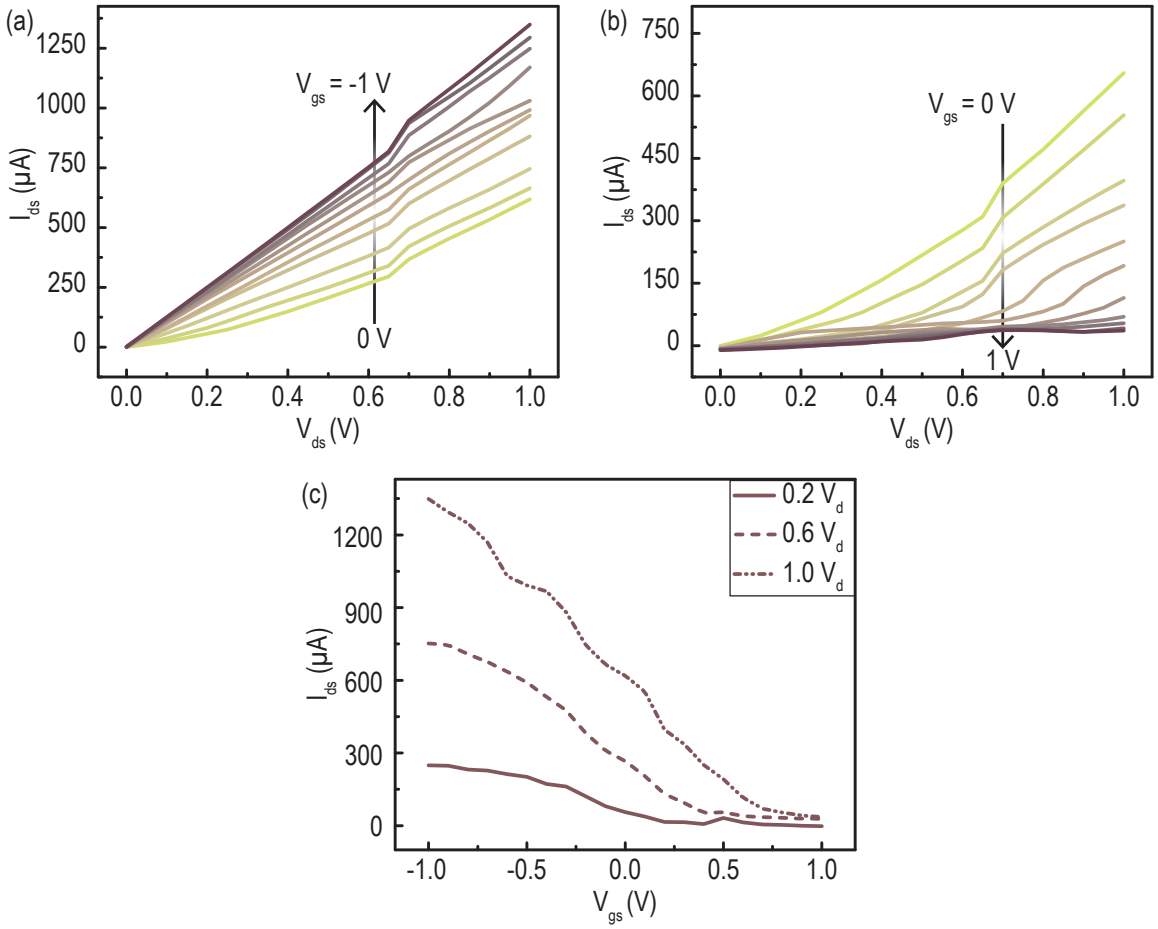

Figure 3.1. Output characteristics of OECT with a PEDOT:PSS channel operating with 0.1 M KCl (aq) recorded for 0 to -1 V of V_{gs} (a) and 0 to -1 V of V_{gs} (b) by 0.1 V steps while sweeping the V_{ds} between 0 and 1 V with intervals of 0.05 V. The transfer I_{ds} vs V_{gs} curve created for the fixed V_{ds} as 0.2, 0.6, 1 V (c)

Figure 3.2 shows repeated measurements under negative and positive gate bias. For the two selected negative magnitudes of V_{gs}, the drastic decrease in the I_{ds} from first to 4^{th} trial is noticeable when the data of four consecutive trials are overlayed (Figure 3.2a,b). The drop in the I_{ds} is about 88 % for either -0.6 V_{gs} or -0.2 V_{gs} when the drain voltage fixed at 0.6 V. This current drop implies that de-doped surface cannot be restored to its initial (doped) state for each measurement, in other words, some of the PEDOTs in the channel cannot be oxidized so it cannot be completely doped (Figure 3.2a, b). In this case, some of the sulfonate ions of PSS^- or chloride ions of electrolyte pushed into the channel might be compensated by other elements in the channel. On the other hand, in figure 3.2c,

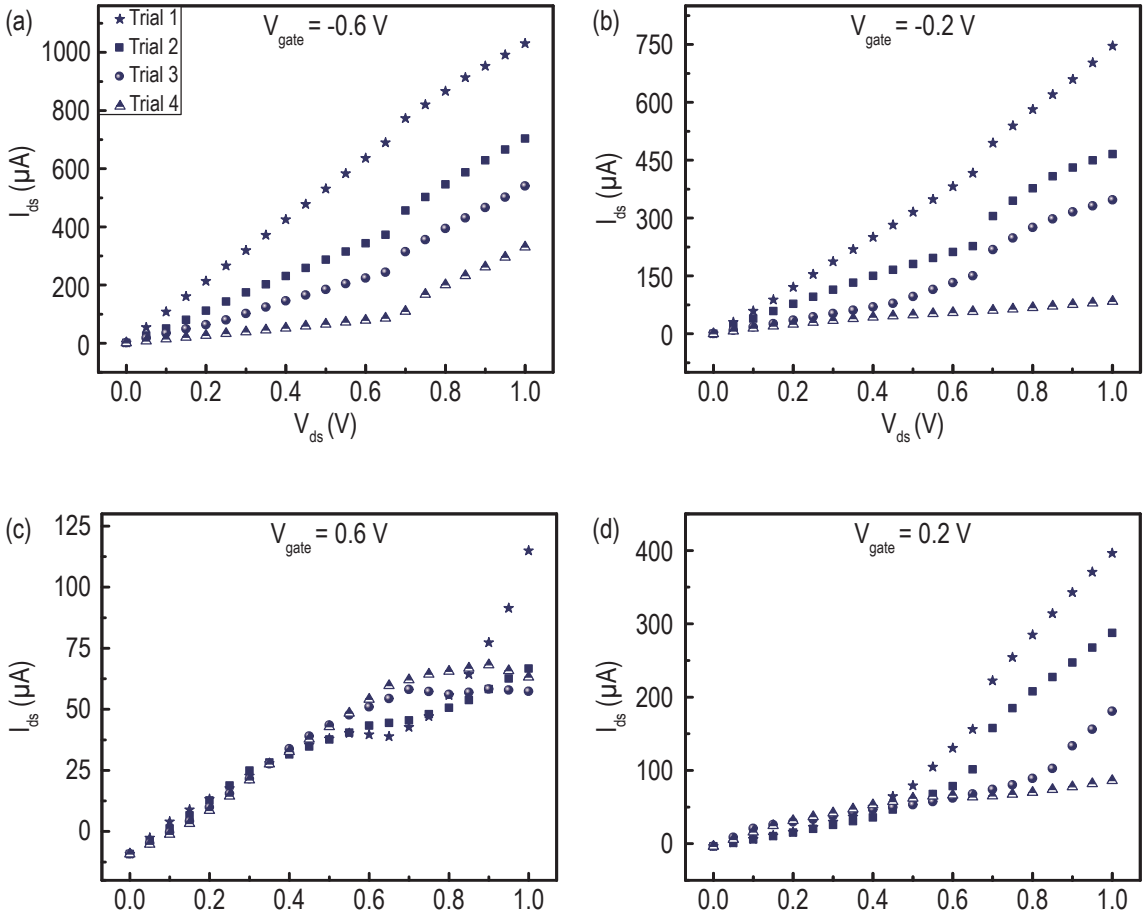

Figure 3.2. Transfer curves of OECT with a PEDOT:PSS channel are plotted by overlaying four consecutive trials of positive (a,c) and negative (b,d) gate bias. Operation parameters are the same as in Figure 3.1.

d, for positive V_{gs}, the change in the current depends of the V_{ds} range for the four trials. While there is no significant change up to 0.45 V of V_{ds}, there is no regular trend at values between 0.45 and 1 V of V_{ds}. For instance, if V_{ds} fixed at 0.65 V, there will be the raise close up to 54 % at 0.6 V of V_{gs} and 59 % decrease at 0.2 V of V_{gs} can be seen. However, I_{ds} values for 4 trials are very close when V_{ds} is held in the range of 0 to 0.45 V and V_{gs} is fixed at 0.6 or 0.2 V. This indicates that the device is reproducible under positive gate bias and lower drain voltages (0-0.45 V).

In order to understand the effect of composition of electrolyte on gating, three different featured dopant molecules shown in figure 3.3 were used separately as a mixture with 0,1 M KCl (aq) in the ratio of 1:10 by weight. OXONE is known as a very good

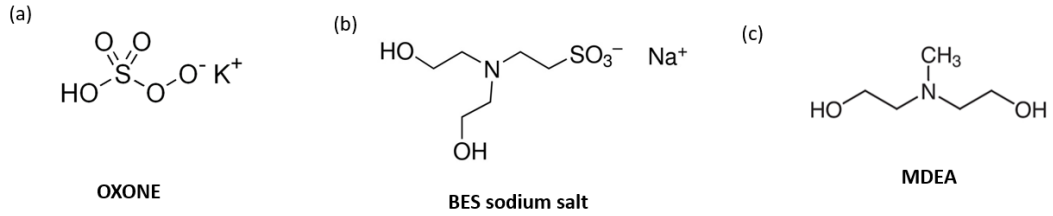

Figure 3.3. Chemical structures of various dopant molecules (a) OXONE, (b) BES Sodium salt, (c) MDEA used for electrolytes of OECT. The combinations of electrolytes are specified in section 3.

oxidizing agent for organic synthesis.[73] In addition, the study of Van der Pol, T. P. et al., propose that aliphatic amine derivatives comprise efficient de-doping of PEDOT:PSS.[74] Moreover, sodium salts are also preferred as counterions in OECT electrolytes.[75] The measurements made with these co-ions will be discussed later in this section.

In Figure 3.4, in the V_{ds} range between 0 and 0.6 V, more stable current response can be obtained similar with the condition of KCl. Although the raise in the I_{ds} is at least two times (Figure 3.4a) when gating from 0 to -1 V, there is a noticeable decay in I_{ds} at least 12 times from V_{gs}= 0 V to 1 V (Figure 3.4b). In addition, in the V_{ds} range between 0.6 and 1 V, the raise in the current response indicates that the surface is no longer reduced (de-doped), which can be explained by the diffusion of cations sent to the channel back into the electrolyte (Figure 3.4b). Furthermore, the transfer curve in Figure 3.4c represents that most efficient gating can be achieved keeping the drain voltage lower than 1 V and gate voltage between -0.5 to 0.5 V.

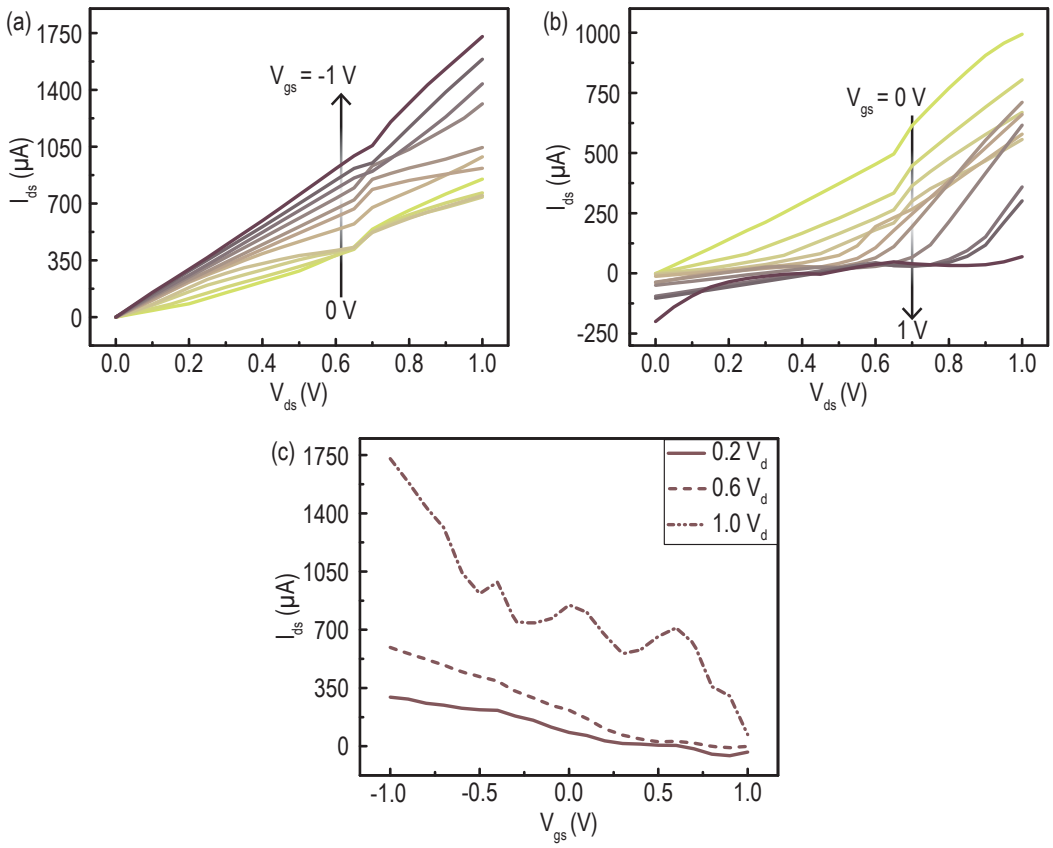

Figure 3.4. Output curves of OECT with a PEDOT:PSS channel operating with a mixture of 0.1 M KCl (aq) & 10% wt OXONE recorded for 0 to -1 V of V_{gs} (a) and 0 to -1 V of V_{gs} (b) by 0.1 V steps while sweeping the V_{ds} between 0 and 1 V with intervals of 0.05 V. The transfer I_{ds} vs V_{gs} curve created for the fixed V_{ds} as 0.2, 0.6, 1 V (c)

As it can be seen in Figure 3.5a, the output characteristic of KCl & BES Sodium salt for negative gate bias similar with KCl and KCl & OXONE. The increase in the I_{ds} is at least two times when V_{gs} applied 0 to -1 V. In Figure 3.5b, the I_{ds} values are closer to zero at V_{gs} lower than 0.4 V and V_{ds} lower than 0.6 V. Still, there is an increase of I_{ds} in the negative direction if V_{gs} higher than 0.4 V. Furthermore, the current response close up to zero at higher gate voltages if the drain voltage sweeps between 0.6 V to 1 V. Overall, the decrease in I_{ds} is four times from V_{gs}= 0 to 1 V. It can be concluded that the de-dope efficiency of KCl & BES Sodium salt mixture is not sufficient as compared to KCl & OXONE, KCl & MDEA and KCl only. If operating conditions set as the magnitude of V_{gs} and V_{ds} are both lower than 0.6 V an efficient gating could be achieved.

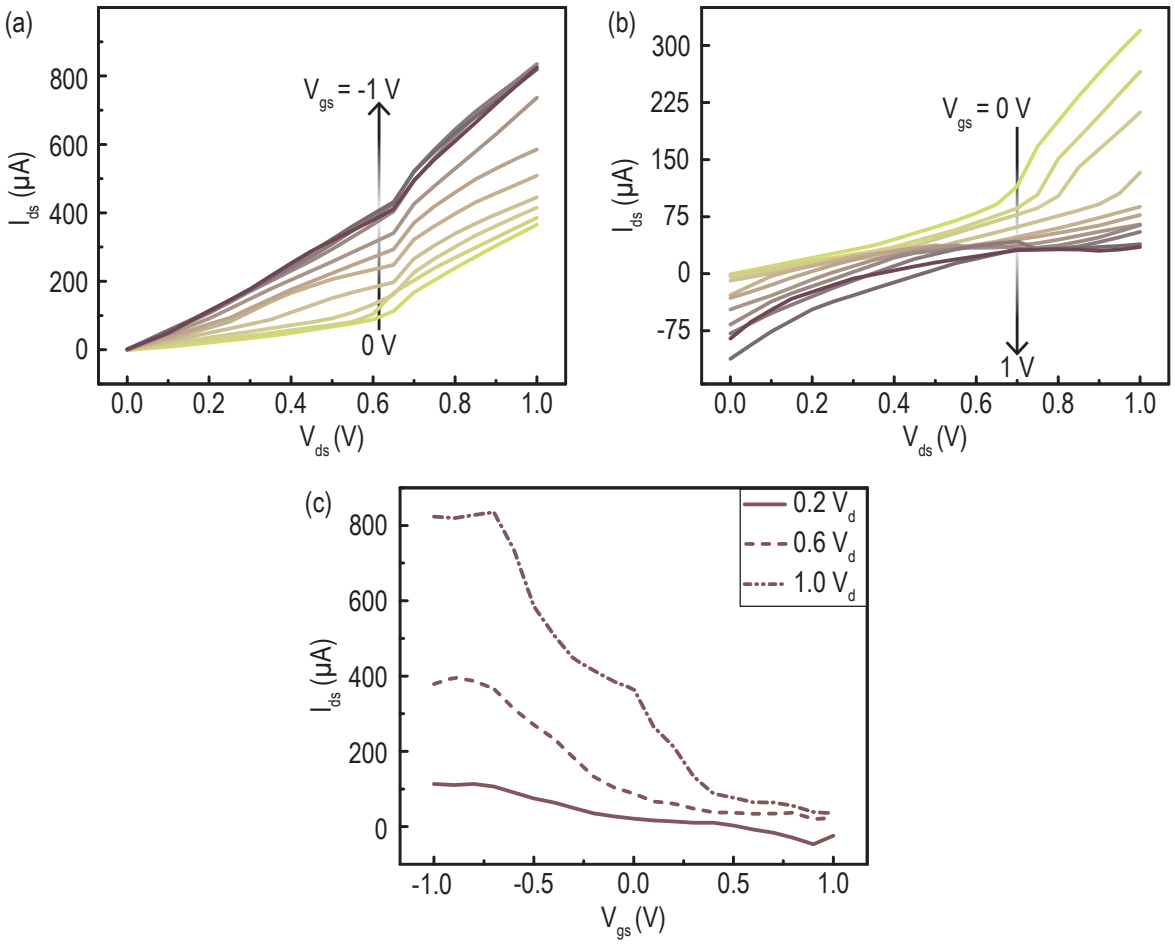

Figure 3.5. Output curves of OECT with a PEDOT:PSS channel operating with a mixture of 0.1 M KCl (aq) & 10% wt BES Sodium salt recorded for 0 to -1 V of V_{gs} (a) and 0 to -1 V of V_{gs} (b) by 0.1 V steps while sweeping the V_{ds} between 0 and 1 V with intervals of 0.05 V. The transfer I_{ds} vs V_{gs} curve created for the fixed V_{ds} as 0.2, 0.6, 1 V (c)

A similar trend to other electrolytes also applies to the KCl & MDEA mixture that showed competitive gating ability with other specimens. While the V_{gs} goes from 0 to -1 V, the current increases by at least three times, while going from 0 to 1 V, the current decreases by at least six times. As discussed in previous dopants, lower gate and drain voltages are necessary to have stable I_{ds} response and adequate gating also for KCl & MDEA.

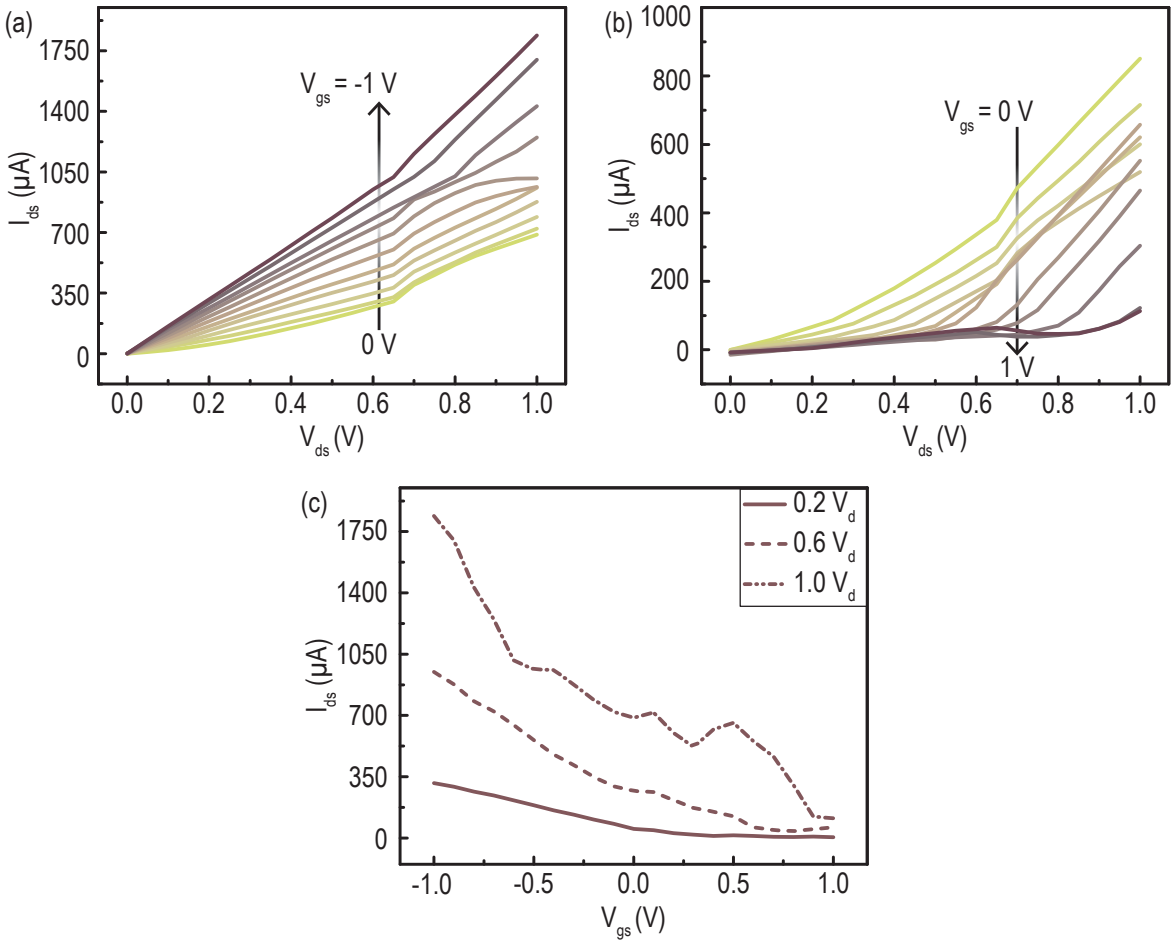

Figure 3.6. Output curves of OECT with a PEDOT:PSS channel operating with a mixture of 0.1 M KCl (aq) & 10% wt MDEA recorded for 0 to -1 V of V_{gs} (a) and 0 to -1 V of V_{gs} (b) by 0.1 V steps while sweeping the V_{ds} between 0 and 1 V with intervals of 0.05 V. The transfer I_{ds} vs V_{gs} curve created for the fixed V_{ds} as 0.2, 0.6, 1 V (c)

In order to better understand the effect of electrolyte composition, different electrolyted OECTs operated in the same conditions were compared (Figure 3.7). Normalized data were overlayed at selected gate biases. It can be seen that the pairs of electrolytes that KCl-KCl& BES and KCl& MDEA-KCl& OXONE exhibit the closest behavior to each other at both positive and negative gate bias. The figure 3.7 illustrates the contribution of co-ions to the electrical properties of the standard device. At 0.6 and -0.6 V_{gs} OXONE and MDEA co-ions contribute positively to the ionic conduction on the other hand BES co-ion did not generate significant affects as compared to the KCl. At -0.6 and -0.2 V_{gs} Oxone and MDEA co-ions act as mediator that facilitating ion mobility. As seen in figure 3.7b

and d, all co-ions contribute ionic conductivity.

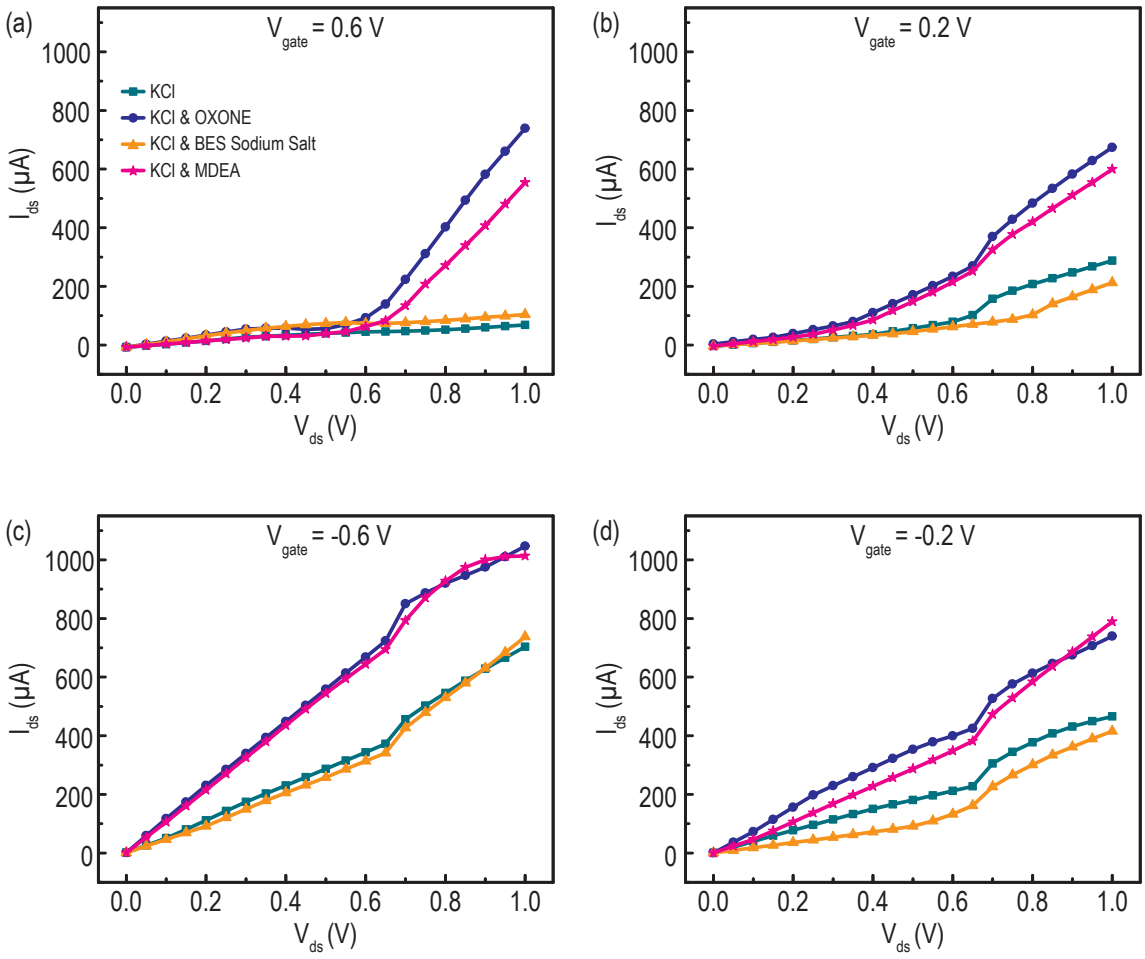

Figure 3.7. Transfer curves of OECT with a PEDOT:PSS channel are plotted by overlaying the responses of various electrolytes under application of positive (a, b) and negative (c, d) gate bias. Operation parameters are the same for each electrolyte.

The figure 3.7 illustrates the contribution of co-ions to the electrical properties of the standard device. At 0.6 and -0.6 V_{gs} OXONE and MDEA co-ions contribute positively to the ionic conduction on the other hand BES co-ion did not generate significant affects as compared to the KCl. At -0.6 and -0.2 V_{gs} Oxone and MDEA co-ions act as mediator that facilitating ion mobility. As seen in figure 3.7b and d, all co-ions contribute ionic conductivity.

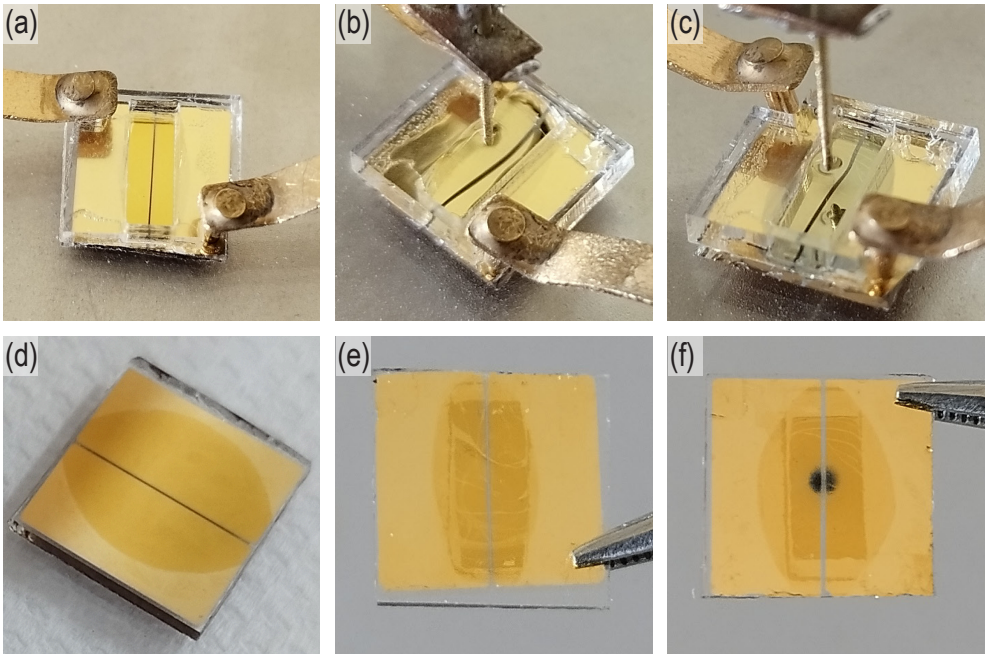

Figure 3.8. The photograph of un-doped surface with and without PMMA-cell (a,d), doping the surface with -0.6 V gate bias (b), de-doping the surface with 0.6 V gate bias (c), doped (e) and de-doped (f) surfaces at dried state after cleaning with Mili-Q water

Besides its electrical properties, it was observed that the color of the PEDOT:PSS thin film is tuned depending on the applied gate bias. This electro-optical feature is defined as the electrochromorphism. Figure 3.8 shows digital images of the device PEDOT:PSS thin film at neutral (un-doped), doped (oxidized) and de-doped (reduced) state during and after OECT measurement. Figure 3.8a and d demonstrate that the film looks transparent when its un-doped (the state where PEDOT's are initially doped with PSS). In figure 3.8b and e, after application of negative gate bias (doped state), the film looks transparent. However, figure 3.8c shows when positive gate bias applied the color of the film changed to blue. In this case, the color of the film changed from blue to transparent the point at which the gate bias removed. Yet, there is a blue spot remains due to overoxidation of PEDOT:PSS.[24,76]

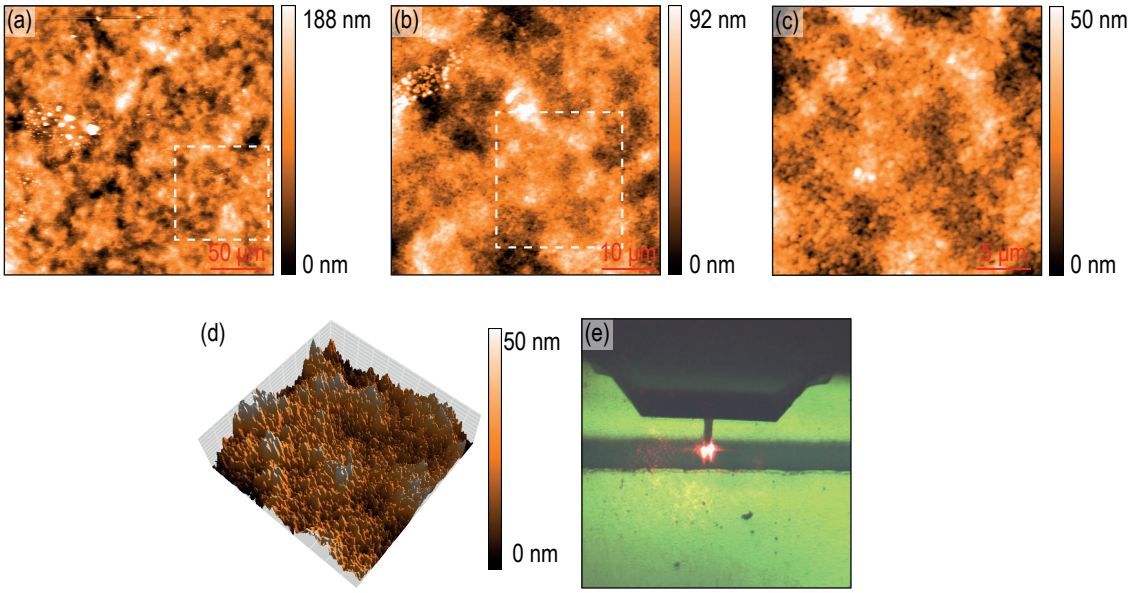

Figure 3.9. AFM topography images for the scanned area of 50 μm (a), 10 μm (b), 5 μm (c) of PEDOT:PSS films and 3D map of 5 μm surface (d) (dashed square lines indicate selected areas for the next scan)

Figure 3.9 shows the AFM height images (50 μm (a), 10 μm (b), 5 μm (c)) and 3D view of the un-doped surface. Consisted with the literature, in figure3.9c the PEDOT domains with luminous PSS clusters can be seen.[60,77,78] In addition 3D view of the 5 μm area given in figure 3.9d. By looking topography images, it is understood that a homogeneous surface functionalization is achieved. Although scanning could not be performed from the exact same points, the difference in surface morphology is could be understood. Figure 3.10 shows that PSS concentration is increased at doped state while decreasing at de-doped condition and de-doping of the sample increases the surface roughness.

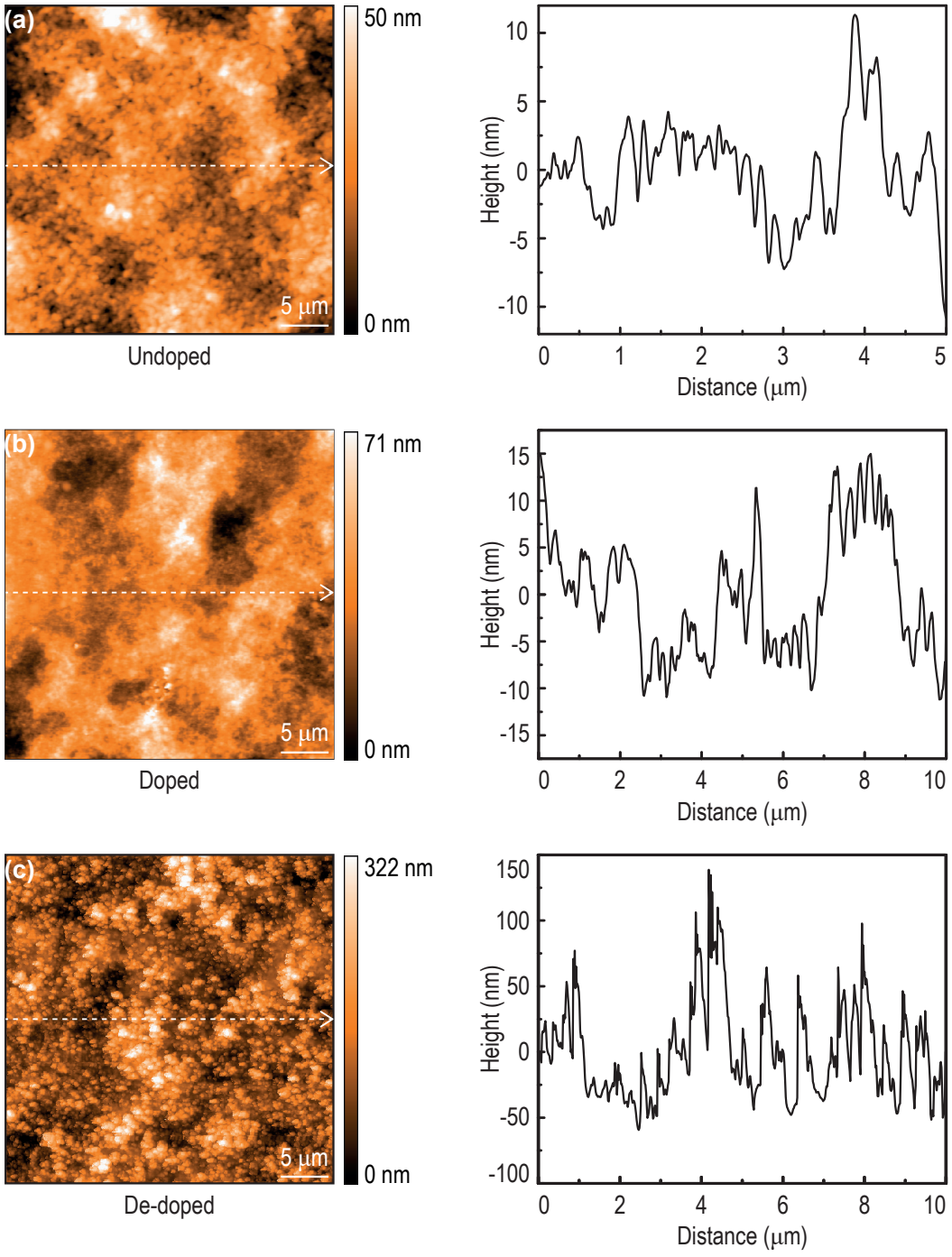

Figure 3.10. AFM topography images and cross sections of un-doped (a), doped (b) , de-doped (c) PEDOT:PSS films for 5μm scanned area

For further insight into the structural changes in PEDOT:PSS thin film at un-doped, doped and de-doped state, surfaces were analyzed by X-Ray Photoelectron Spectroscopy (XPS). The preparation of sample and dope & de-doping process were mentioned in previous sections (2.2.2, 2.3.1) and parameters of XPS analyses are given in section 2.3.2. Figure 3.11 presents the XPS spectra of C1s, O1s and S2p. Compared to the un-doped state while the peak intensity at 285.0 eV (aliphatic carbons, C=C) and 289.0 eV (C=O and derivatives[76,79]) increases in the doped state, a decrease is seen in the peak at 286.0 eV, which represents the C-O-C bonds (Figure 3.11a,b). In addition, an increase in the peak at 289.0 eV is observed in the doped state. This change can be explained by the neutral PEDOT's transition to a bipolaron (dication; doped) state which stabilized by the ionic bond formed with PSS- in the channel or chlorine anions injected into the channel. The neutral and bipolaron PEDOT structures are present in Figure 3.12. The peak at 289.0 eV corresponds to C=O-C group in the bipolaron PEDOT resonance structure (Figure 3.12b), and the increase in peak intensity at this point proves the presence of bipolaron PEDOTs on the doped surface. In Figure 3.11c, a decrease is seen in the ratio of aliphatic carbons to aromatics. In the de-doped state, the sulfonate units of PSS are compensated by potassium ions sent to the channel via ionic bonds that results in a reduction of peak intensity at 285.0 eV. Moreover, the raise in the amount of C=O bonds (289.0 eV) and decrease in the aliphatic carbons (285.0 eV) could be resulted by the oxidation of the PEDOT chain (Figure 3.11c).

On the other hand, the peaks seen about 5.0 eV beyond the main C1s peaks in figures 3.11b and 3.11c are aromatic moieties, which are also called $\pi \rightarrow \pi^*$ shake-up satellites in the literature.[80,81] The spectra with $\pi \rightarrow \pi^*$ satellite are similar to the polystyrene sulfonate (PSS) spectra as given in the XPS database[79]. To the study of Pignataro et al., charge-transfer type of shake-up peaks disappear in saturated form of aromatic species.[82].The photoelectron binding energy values for C1s were given in Table 3.1.

Table 3.1. XPS binding energies of C1s [76,79,83]

Chemical structure	Binding Energy (eV)
C=C	284.5
C-C, C-H, C-S	284.8 - 285.0
C-O, C-O-C	286.0 - 286.7
C=O	287.8 - 288.3
O-C=O	288.5 - 289.5

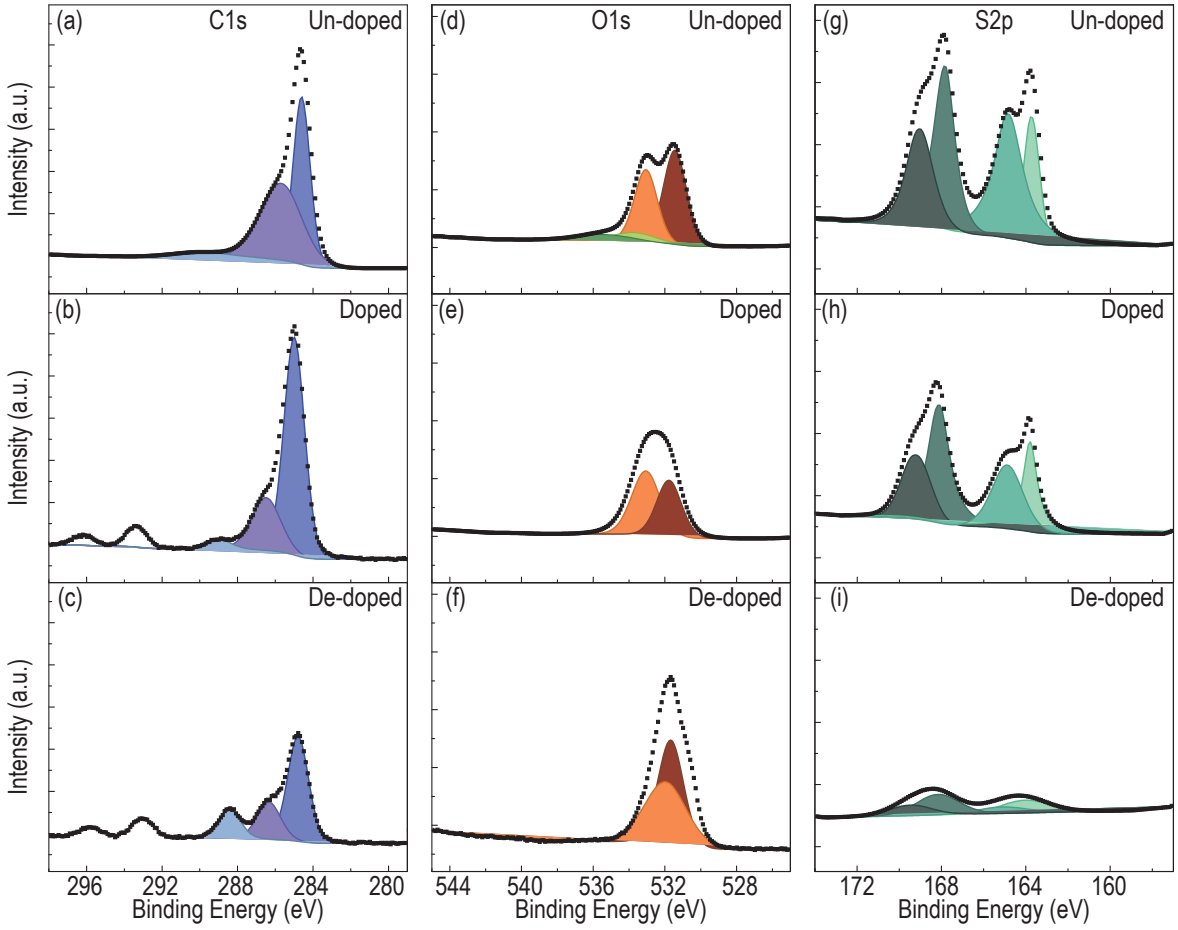

Figure 3.11. XPS spectra of deconvoluted C1s, O1s and S2p of un-doped, doped and de-doped PEDOT:PSS thin film

In Figure 3.11d, e and f, O1s spectra are plotted for the un-doped, doped, de-doped states, respectively. According to G. Greczynski et al, in the O1s photoelectron spectra of PEDOT:PSS, 533.7 eV corresponds oxygen atoms in the dioxyethylene group of PEDOT, 531.7 eV comprises the oxygen atoms in the sulfonate group in the PSS^-.[84] Besides, to the XPS database[79] there are also other species present in that range such as aliphatic C-O-C (532.5 eV) and aromatic C-O-C (533.3 eV). In Figure 3.11d,e,f shows different ratios of these two distinct peaks near 532.0 and 533.0 eV. When un-dope and dope state are compared, it can be seen that there is a difference between peak ratios. The peak intensity at 533.3 eV is greater than that at 532.5 eV, indicating an increase in aromatic C-O-C structure. Complementary to the finding in the C1s spectra, this result supports the presence of the bipolaron PEDOT structure. The possible oxygen atoms at 532.5 and 533.1 eV located in the structure of neutral and bipolaron PEDOT are labeled in Figure 3.12.

On the other hand, there is a shift to the higher energy of 0.4 eV from the un-doped state to the doped state. This shift might be caused by the electronegativity of chlorine atoms sent to the channel in the doping process. In this case, chlorine can form a stronger bond with oxygen than with sulfur atoms, so that the oxygen core electrons are more strongly attracted by the nucleus and causing an increase in their binding energies.[62] However, there is a shift to lower energy of 0.9 eV from the doped state to the de-doped state which might be originated by coulombic attraction of potassium ions with PSS^-. The peak at 532.9 eV shifted to lower BE (532.0 eV) may indicate the formation of SO_2C (sulfone) groups on PEDOT.[76] The core level of O1s binding energies of possible chemical structures are given at Table 3.2.

Table 3.2. XPS binding energies of O1s[79,83]

Chemical structure	Binding Energy (eV)
C-O-C (aliphatic)	532.5
C-O-C (aromatic)	533.3
SO_4^{2-}	532.2
ClO_4^-	532.6 - 533.0
C-OH (aliphatic)	532.8
C-OH (aromatic)	533.6
C=O (aromatic)	531.5
C=O (aliphatic)	532.3
Epoxide	533.1

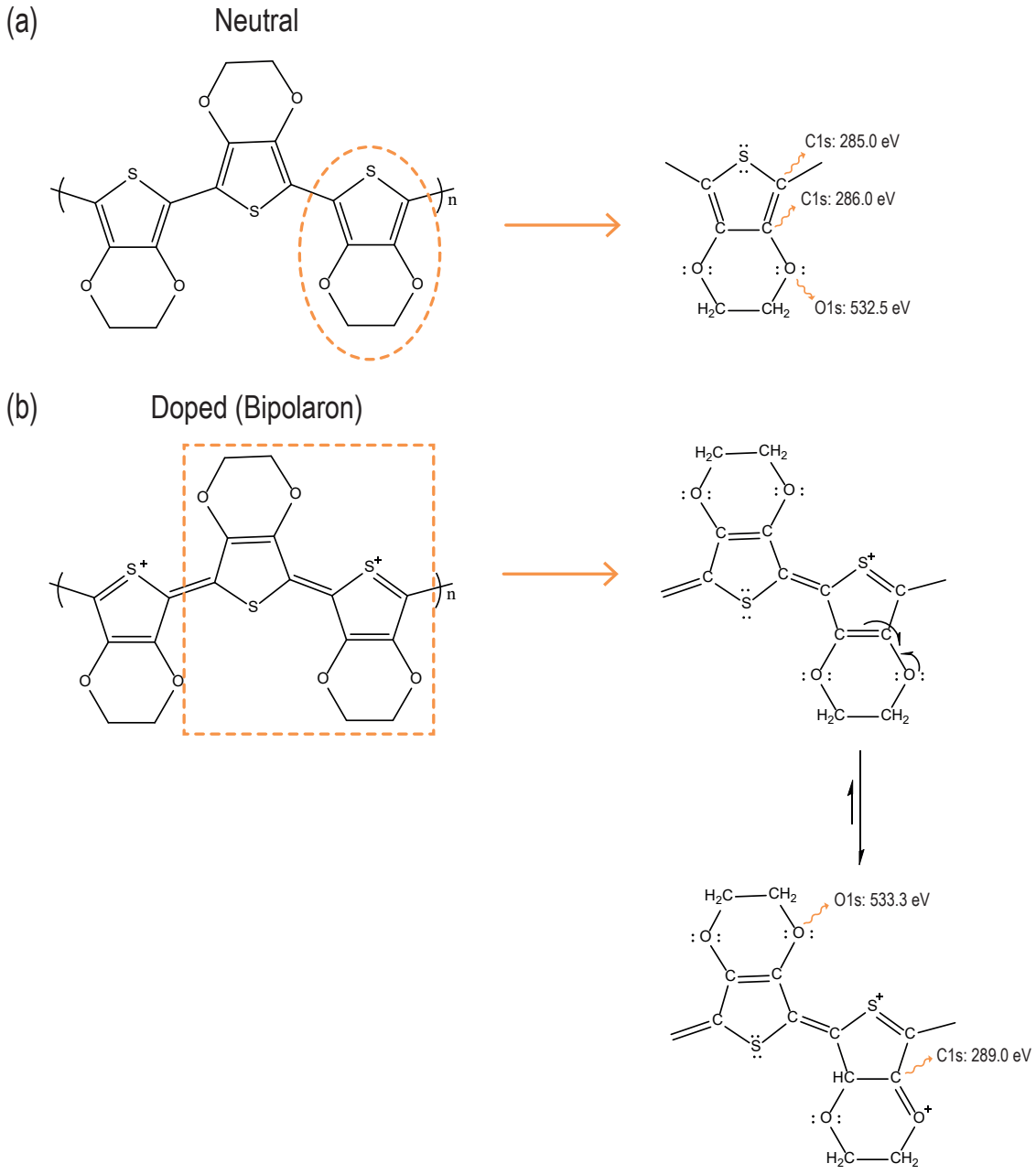

Figure 3.12. Neutral and doped structure of Poly(3,4-ethylenedioxythiophene) (PEDOT). A resonance structures of doped $PEDOT^{+}$ are shown and C1s (285.0, 286.0 eV) and O1s (532.5, 533.1 eV) binding energies are labeled.

The core level S2p photoelectron spectra recorded for un-doped, doped, de-doped film are shown in Figure 3.11g, h, i and XPS binding energies given in the literature are listed in Table 3.3. The envelope of S2p spectrum originally consist of two doublets ($2p_{1/2}$, $2p_{3/2}$) due to its spin-orbit coupling.[84] At first glance, it can be understood that the same species are present even if there are minor shifts between the three spectra, however a significant decrease in intensity is notable while transitioning from the un-dope to the de-dope state. The doublet which represents sulfur atom in PEDOT appears at lower BE's and the sulfur atom in PSS defined by following doublet at higher BE's. Due to the electronegativity of the oxygens in the sulfonate group, the electron density of sulfur atoms in PSS is reduced compared to those in PEDOT, resulting in a difference in their BE. When examined in more detail, although no significant shift was observed in the binding energies of the PEDOT peaks, a 0.3 eV shift to higher energy was observed in the peaks indicating the sulfonate groups in PSS when transitioning from un-dope to dope state. The shift could be resulted by contribution of the chlorine atom into the channel during the doping process, increasing electronegativity of the PSS cause a raise in the BE of sulfur atoms.

Table 3.3. XPS binding energies of S2p[79,83]

Chemical structure	Binding Energy (eV)
C-S-C	163.7
C-S-H	163.8
C_4S-H	164.0
C-SO_3H, C-SO_3Na	168.1
Metal sulfate	169.0

The Cl(2p) and K(2p) photoelectron spectra were also recorded for a better examination of the dope and de-dope processes (Figure 3.13). As listed literature BE values in Table 3.4 and 3.5, XPS spectra of Cl(2p) consist of two species as Cl atoms from KCl (198.6 eV (a), 199.0 eV (b)) and chlorobenzene (200.2 eV (a), 200.6 eV (b)).

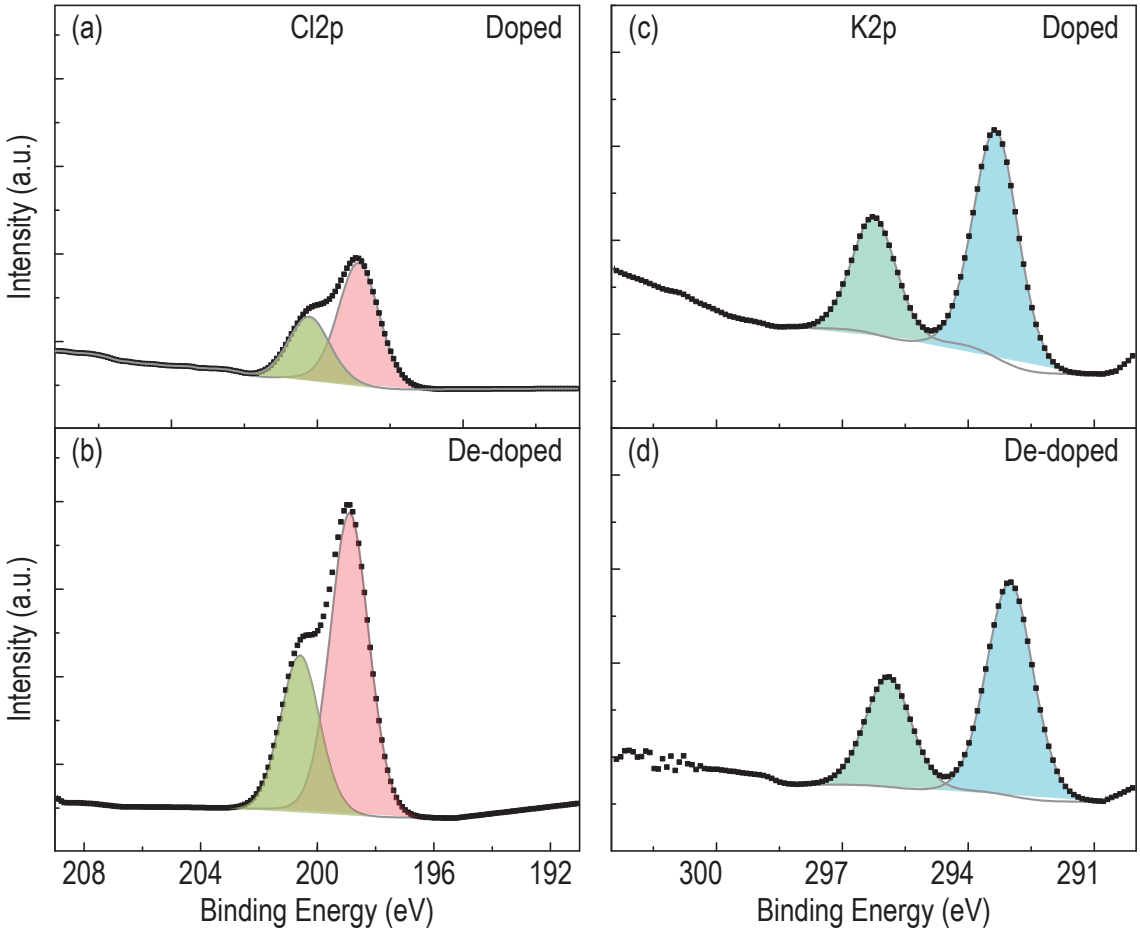

Figure 3.13. The XPS spectra of deconvoluted Cl2p and K2p of doped and de-doped PEDOT:PSS thin film

In Figure 3.13c and d, potassium spectra split into two distinct peak that one is identified as K atoms from KCl (293.4 eV (c), 293.0 eV (d)) and K^+ (296.3 eV (c), 295.9 eV (d)).[85] Although there is no significant species-specific difference in dope and de-dope state, the shifts in BE's may indicate the difference in the surface structure. From dope to de-dope state, 0.4 eV shift to higher energy is seen in Cl(2p) spectrum, while 0.3 eV shift to lower energy is seen in K(2p) spectrum. The shifts in the binding energies may be related to the electronegativity differences of the bonds in the newly formed species with

Table 3.4. XPS binding energies of Cl2p[83]

Chemical structure	Binding Energy (eV)
KCl	198.6 - 198.9
C_6H_5Cl	200.2 - 200.6

Table 3.5. XPS binding energies of K2p[83,85]

Chemical structure	Binding Energy (eV)
KCl,$KClO_3$, $KClO_4$	292.3-293.4

Cl and K. In order to better interpretation the position of ions on the substrate surface, this section will be continued with the XPS mapping analysis results.

Figure3.14 shows the XPS mapping of C, S, O, K atoms on the surface through their chemical abundances. It can be seen that the amount of C, S, O atoms attached uniform to the surface at un-dope state changes with the presence of new species at dope state. At de-dope state oxygen atoms located on the center of the semiconductor channel however carbon and sulfur atoms clustered towards the corners of the channel. The raise in the oxygen concentration at this point could be caused by the oxidation of the PEDOT. As discussed previously, the over-oxidized area in de-dope surface (figure 3.8f) could also be confirmed by chemical map of oxygen. Furthermore, to investigate the counter-ion movement, chemical maps of potassium ions at doped and de-doped state were compared. In doped state, potassium ions dispersed homogeneously on the surface, however they located far from the center of the channel in the de-dope state, and this can be expressed by the migration of potassium cations injected into the channel under positive gate bias.

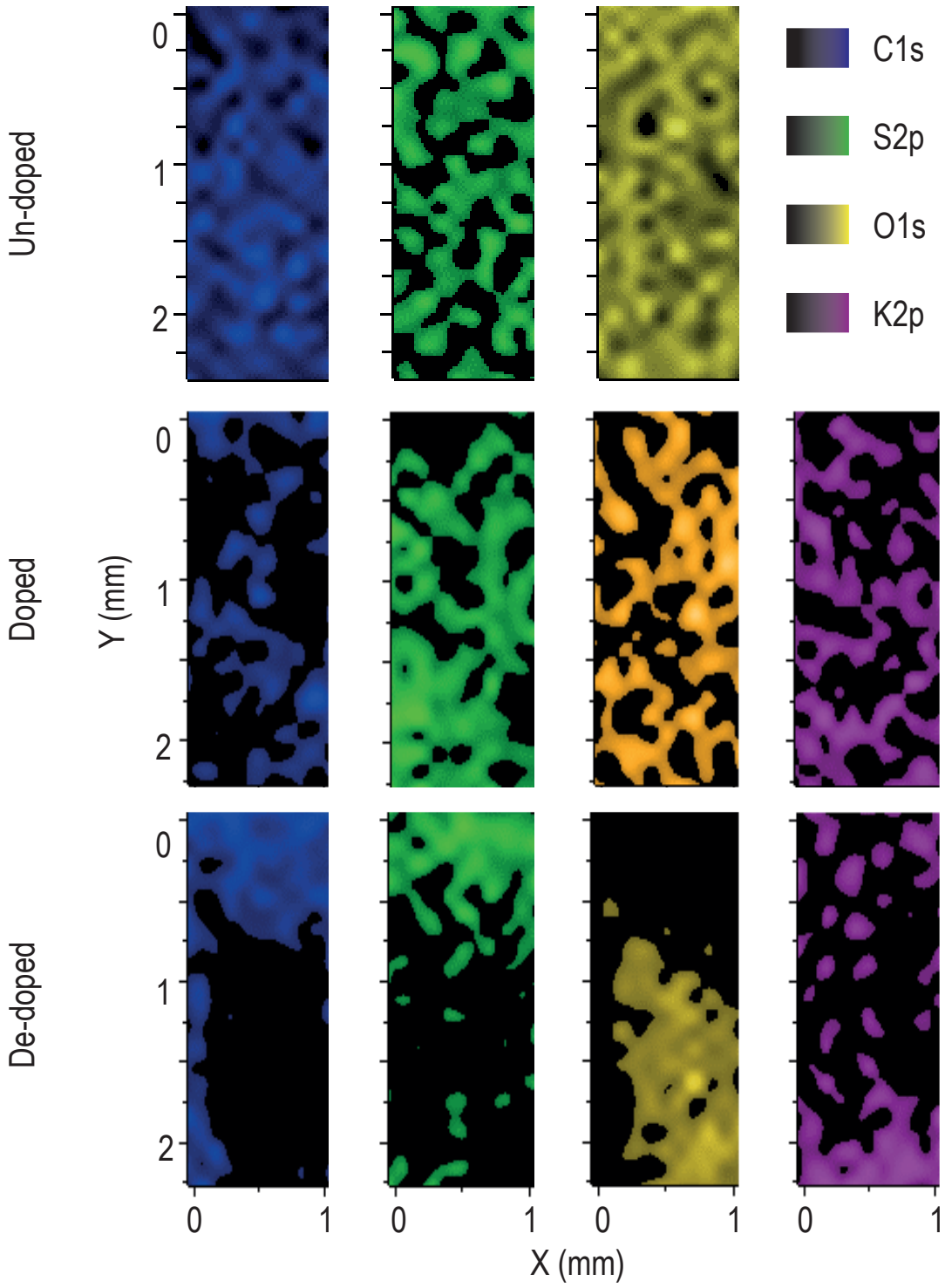

Figure 3.14. XPS chemical mapping of C1s (blue), S2p (green), O1s (yellow), K2p (purple) atoms on the channel surface for un-doped, doped, and de-doped samples

CHAPTER 4

CONCLUSION

In this work, the properties of ion transport in organic electrochemical transistors (OECTs) were studied. For OECT application, PEDOT:PSS was preferred for an organic active channel, as an example to p-type dope conjugated polyelectrolytes working in depletion mode and because of its conductivity and morphological advantages. In order to interpret the mixed ion to electron transport, both electrical and structural characterization were performed. The electrical characterization was done using KCl(aq) and its aqueous solutions with three different co-ions. In the characterization, the most efficient range of our depletion-mode OECT device was determined as 0 to 0.45 V for drain voltage and 0 to $\pm$ 0.6 V for gate voltage to prevent responses resulted by the faradaic processes. When the repeatability of the device is examined, it was seen that the appropriate drain voltage range for an sufficient gating is between 0 and 0.45 V. However, a reduction of up to eighty percent in redoping efficiency has been found, and it has been suggested that this may be due to the change in PEDOT conformation, the reduction of doping efficiency by PSS compensated by other species, and the irreversible overoxidation process. Considering the effect of ion composition, it was decided that BES sodium salt did not have a notable contribution to the gating performance compared to OXONE and MDEA. Yet all co-ions promote to ion conduction.

In addition to the above-mentioned findings, the electrochromic property of PEDOT:PSS was also demonstrated separately for the un-doped dope, de-dope state in this experimental study (Figure3.8). Besides, the morphological changes in un-dope, dope and de-dope state were analyzed by AFM height imaging. Unlike the un-doped state, it was observed that the luminous dot density increased slightly in the dope state, while the decreased in the de-dope state.

The study was continued with X-ray Photoelectron spectroscopy, which reveals the change in the active channel structure caused by ion injection. C(1s), O(1s) and S(2p) core level spectra proved that the density of bipolaron structures increased on the surface of the PEDOT:PSS film after redoping in the presence of electrolyte by negative gate bias modulation, and then when it becomes de-dope state with positive gate bias, there

is a transition from the structures of bipolaron to the neutral PEDOT. Complementary to the XPS survey spectra, the presence, density and location of ions in the channel were visualized by XPS mapping. According to the mapping results, it was concluded that the potassium ions injected into the channel were pushed towards the channel edges under positive gate bias.

REFERENCES

(1) Guo, X.; Facchetti, A. The journey of conducting polymers from discovery to application. *Nature Materials* **2020**, *19*, 922–928.

(2) Zeglio, E. Self-doped conjugated polyelectrolytes for bioelectronics applications. Ph.D. thesis, Linköping University Electronic Press, 2016.

(3) Fahlman, M.; Fabiano, S.; Gueskine, V.; Simon, D.; Berggren, M.; Crispin, X. Interfaces in organic electronics. *Nature Reviews Materials* **2019**, *4*, 627–650.

(4) Gharahcheshmeh, M. H.; Gleason, K. Texture and nanostructural engineering of conjugated conducting and semiconducting polymers. *Materials Today Advances* **2020**, *8*, 100086.

(5) Groenendaal, L.; Jonas, F.; Freitag, D.; Pielartzik, H.; Reynolds, J. R. Poly (3, 4-ethylenedioxythiophene) and its derivatives: past, present, and future. *Advanced materials* **2000**, *12*, 481–494.

(6) Rivnay, J.; Inal, S.; Collins, B. A.; Sessolo, M.; Stavrinidou, E.; Strakosas, X.; Tassone, C.; Delongchamp, D. M.; Malliaras, G. G. Structural control of mixed ionic and electronic transport in conducting polymers. *Nature communications* **2016**, *7*, 1–9.

(7) Sun, K.; Zhang, S.; Li, P.; Xia, Y.; Zhang, X.; Du, D.; Isikgor, F. H.; Ouyang, J. Review on application of PEDOTs and PEDOT: PSS in energy conversion and storage devices. *Journal of Materials Science: Materials in Electronics* **2015**, *26*, 4438–4462.

(8) Fan, J.; Rezaie, S. S.; Facchini-Rakovich, M.; Gudi, D.; Montemagno, C.; Gupta, M. Tuning PEDOT: PSS conductivity to obtain complementary organic electrochemical transistor. *Organic Electronics* **2019**, *66*, 148–155.

(9) Rivnay, J.; Leleux, P.; Sessolo, M.; Khodagholy, D.; Hervé, T.; Fiocchi, M.; Malliaras, G. G. Organic electrochemical transistors with maximum transconductance at zero gate bias. *Advanced Materials* **2013**, *25*, 7010–7014.

(10) Zhang, S.; Kumar, P.; Nouas, A. S.; Fontaine, L.; Tang, H.; Cicoira, F. Solvent-induced changes in PEDOT: PSS films for organic electrochemical transistors. *APL materials* **2015**, *3*, 014911.

(11) Keene, S. T.; van der Pol, T. P.; Zakhidov, D.; Weijtens, C. H.; Janssen, R. A.; Salleo, A.; van de Burgt, Y. Enhancement-Mode PEDOT: PSS Organic Electrochemical Transistors Using Molecular De-Doping. *Advanced Materials* **2020**, *32*, 2000270.

(12) Mantione, D.; Del Agua, I.; Schaafsma, W.; ElMahmoudy, M.; Uguz, I.; Sanchez-Sanchez, A.; Sardon, H.; Castro, B.; Malliaras, G. G.; Mecerreyes, D. Low-temperature cross-linking of PEDOT: PSS films using divinylsulfone. *ACS applied materials & interfaces* **2017**, *9*, 18254–18262.

(13) Ouyang, J. "Secondary doping"methods to significantly enhance the conductivity of PEDOT: PSS for its application as transparent electrode of optoelectronic devices. *Displays* **2013**, *34*, 423–436.

(14) Fan, B.; Mei, X.; Ouyang, J. Significant Conductivity Enhancement of Conductive Poly(3,4-ethylenedioxythiophene):Poly(styrenesulfonate) Films by Adding Anionic Surfactants into Polymer Solution. *Macromolecules* **2008**, *41*, 5971–5973.

(15) Yi, C.; Wilhite, A.; Zhang, L.; Hu, R.; Chuang, S. S.; Zheng, J.; Gong, X. Enhanced thermoelectric properties of poly (3, 4-ethylenedioxythiophene): poly (styrenesulfonate) by binary secondary dopants. *ACS applied materials & interfaces* **2015**, *7*, 8984–8989.

(16) Zhu, Z.; Liu, C.; Xu, J.; Jiang, Q.; Shi, H.; Liu, E. Improving the electrical conductivity of PEDOT: PSS films by binary secondary doping. *Electronic Materials Letters* **2016**, *12*, 54–58.

(17) Reyes-Reyes, M.; Cruz-Cruz, I.; López-Sandoval, R. Enhancement of the electrical conductivity in PEDOT: PSS films by the addition of dimethyl sulfate. *The Journal of Physical Chemistry C* **2010**, *114*, 20220–20224.

(18) Döbbelin, M.; Marcilla, R.; Salsamendi, M.; Pozo-Gonzalo, C.; Carrasco, P. M.; Pomposo, J. A.; Mecerreyes, D. Influence of ionic liquids on the electrical conductivity and morphology of PEDOT: PSS films. *Chemistry of materials* **2007**, *19*, 2147–2149.

(19) Yeon, C.; Kim, G.; Lim, J.; Yun, S. Highly conductive PEDOT: PSS treated by sodium dodecyl sulfate for stretchable fabric heaters. *RSC advances* **2017**, *7*, 5888–5897.

(20) Kishi, N.; Kondo, Y.; Kunieda, H.; Hibi, S.; Sawada, Y. Enhancement of thermoelectric properties of PEDOT: PSS thin films by addition of anionic surfactants. *Journal of Materials Science: Materials in Electronics* **2018**, *29*, 4030–4034.

(21) Wu, F.; Li, P.; Sun, K.; Zhou, Y.; Chen, W.; Fu, J.; Li, M.; Lu, S.; Wei, D.; Tang, X.; Zang, Z.; Sun, L.; Liu, X.; Ouyang, J. Conductivity enhancement of PEDOT: PSS via addition of chloroplatinic acid and its mechanism. *Advanced Electronic Materials* **2017**, *3*, 1700047.

(22) Lee, J. H.; Jeong, Y. R.; Lee, G.; Jin, S. W.; Lee, Y. H.; Hong, S. Y.; Park, H.; Kim, J. W.; Lee, S.-S.; Ha, J. S. Highly conductive, stretchable, and transparent PEDOT: PSS electrodes fabricated with triblock copolymer additives and acid treatment. *ACS applied materials & interfaces* **2018**, *10*, 28027–28035.

(23) Yemata, T. A.; Zheng, Y.; Kyaw, A. K. K.; Wang, X.; Song, J.; Chin, W. S.; Xu, J. Modulation of the doping level of PEDOT: PSS film by treatment with hydrazine to improve the Seebeck coefficient. *RSC advances* **2020**, *10*, 1786–1792.

(24) Friedlein, J. T. Device physics and material science of organic electrochemical transistors. Ph.D. thesis, University of Colorado at Boulder, 2017.

(25) White, H. S.; Kittlesen, G. P.; Wrighton, M. S. Chemical derivatization of an array of three gold microelectrodes with polypyrrole: fabrication of a molecule-based transistor. *Journal of the American Chemical Society* **1984**, *106*, 5375–5377.

(26) Rivnay, J.; Inal, S.; Salleo, A.; Owens, R. M.; Berggren, M.; Malliaras, G. G. Organic electrochemical transistors. *Nature Reviews Materials* **2018**, *3*, 1–14.

(27) Lin, P.; Yan, F. Organic thin-film transistors for chemical and biological sensing. *Advanced materials* **2012**, *24*, 34–51.

(28) Strakosas, X.; Bongo, M.; Owens, R. M. The organic electrochemical transistor for biological applications. *Journal of Applied Polymer Science* **2015**, *132*.

(29) Nishizawa, M.; Matsue, T.; Uchida, I. Penicillin sensor based on a microarray electrode coated with pH-responsive polypyrrole. *Analytical chemistry* **1992**, *64*, 2642–2644.

(30) Bernards, D. A.; Macaya, D. J.; Nikolou, M.; DeFranco, J. A.; Takamatsu, S.; Malliaras, G. G. Enzymatic sensing with organic electrochemical transistors. *Journal of Materials Chemistry* **2008**, *18*, 116–120.

(31) Yang, S. Y.; Cicoira, F.; Byrne, R.; Benito-Lopez, F.; Diamond, D.; Owens, R. M.; Malliaras, G. G. Electrochemical transistors with ionic liquids for enzymatic sensing. *Chemical Communications* **2010**, *46*, 7972–7974.

(32) Liao, J.; Lin, S.; Yang, Y.; Liu, K.; Du, W. Highly selective and sensitive glucose sensors based on organic electrochemical transistors using TiO2 nanotube arrays-based gate electrodes. *Sensors and Actuators B: Chemical* **2015**, *208*, 457–463.

(33) Khodagholy, D.; Curto, V. F.; Fraser, K. J.; Gurfinkel, M.; Byrne, R.; Diamond, D.; Malliaras, G. G.; Benito-Lopez, F.; Owens, R. M. Organic electrochemical transistor incorporating an ionogel as a solid state electrolyte for lactate sensing. *Journal of Materials Chemistry* **2012**, *22*, 4440–4443.

(34) Tang, H.; Lin, P.; Chan, H. L.; Yan, F. Highly sensitive dopamine biosensors based on organic electrochemical transistors. *Biosensors and Bioelectronics* **2011**, *26*, 4559–4563.

(35) Berto, M.; Diacci, C.; Theuer, L.; Di Lauro, M.; Simon, D. T.; Berggren, M.; Biscarini, F.; Beni, V.; Bortolotti, C. A. Label free urea biosensor based on organic electrochemical transistors. *Flexible and Printed Electronics* **2018**, *3*, 024001.

(36) Khodagholy, D.; Doublet, T.; Quilichini, P.; Gurfinkel, M.; Leleux, P.; Ghestem, A.; Ismailova, E.; Hervé, T.; Sanaur, S.; Bernard, C.; Malliaras, G. G. In vivo recordings of brain activity using organic transistors. *Nature communications* **2013**, *4*, 1–7.

(37) Gkoupidenis, P.; Schaefer, N.; Garlan, B.; Malliaras, G. G. Neuromorphic functions in PEDOT: PSS organic electrochemical transistors. *Advanced Materials* **2015**, *27*, 7176–7180.

(38) Van De Burgt, Y.; Lubberman, E.; Fuller, E. J.; Keene, S. T.; Faria, G. C.; Agarwal, S.; Marinella, M. J.; Alec Talin, A.; Salleo, A. A non-volatile organic electrochemical device as a low-voltage artificial synapse for neuromorphic computing. *Nature materials* **2017**, *16*, 414–418.

(39) Gkoupidenis, P.; Koutsouras, D. A.; Malliaras, G. G. Neuromorphic device architectures with global connectivity through electrolyte gating. *Nature communications* **2017**, *8*, 1–8.

(40) Nilsson, D.; Robinson, N.; Berggren, M.; Forchheimer, R. Electrochemical logic circuits. *Advanced Materials* **2005**, *17*, 353–358.

(41) Hütter, P. C.; Rothländer, T.; Scheipl, G.; Stadlober, B. All screen-printed logic gates based on organic electrochemical transistors. *IEEE Transactions on Electron Devices* **2015**, *62*, 4231–4236.

(42) Braendlein, M.; Lonjaret, T.; Leleux, P.; Badier, J.-M.; Malliaras, G. G. Voltage amplifier based on organic electrochemical transistor. *Advanced science* **2017**, *4*,

1600247.

(43) Inal, S.; Malliaras, G. G.; Rivnay, J. Benchmarking organic mixed conductors for transistors. *Nature communications* **2017**, *8*, 1–7.

(44) Bernards, D. A.; Malliaras, G. G. Steady-state and transient behavior of organic electrochemical transistors. *Advanced Functional Materials* **2007**, *17*, 3538–3544.

(45) Friedlein, J. T.; McLeod, R. R.; Rivnay, J. Device physics of organic electrochemical transistors. *Organic Electronics* **2018**, *63*, 398–414.

(46) Paudel, P. R.; Tropp, J.; Kaphle, V.; Azoulay, J. D.; Lüssem, B. Organic electrochemical transistors–from device models to a targeted design of materials. *Journal of Materials Chemistry C* **2021**, *9*, 9761–9790.

(47) Sun, H.; Vagin, M.; Wang, S.; Crispin, X.; Forchheimer, R.; Berggren, M.; Fabiano, S. Complementary logic circuits based on high-performance n-type organic electrochemical transistors. *Advanced Materials* **2018**, *30*, 1704916.

(48) Donahue, M. J.; Williamson, A.; Strakosas, X.; Friedlein, J. T.; McLeod, R. R.; Gleskova, H.; Malliaras, G. G. High-Performance Vertical Organic Electrochemical Transistors. *Advanced Materials* **2018**, *30*, 1705031.

(49) Rivnay, J.; Leleux, P.; Ferro, M.; Sessolo, M.; Williamson, A.; Koutsouras, D. A.; Khodagholy, D.; Ramuz, M.; Strakosas, X.; Owens, R. M.; Benar, C.; Badier, J.-M.; Bernard, C.; Malliaras, G. G. High-performance transistors for bioelectronics through tuning of channel thickness. *Science advances* **2015**, *1*, e1400251.

(50) Nielsen, C. B.; Giovannitti, A.; Sbircea, D.-T.; Bandiello, E.; Niazi, M. R.; Hanifi, D. A.; Sessolo, M.; Amassian, A.; Malliaras, G. G.; Rivnay, J.; McCulloch, I. Molecular design of semiconducting polymers for high-performance organic electrochemical transistors. *Journal of the American Chemical Society* **2016**, *138*, 10252–10259.

(51) Kaphle, V.; Liu, S.; Al-Shadeedi, A.; Keum, C.-M.; Lüssem, B. Contact resistance effects in highly doped organic electrochemical transistors. *Advanced Materials* **2016**, *28*, 8766–8770.

(52) Kalkan, S. B. The effect of atmospheric gases on the electrical stability of graphene. Ph.D. thesis, Izmir Institute of Technology (Turkey), 2017.

(53) Pujari, S. P.; Scheres, L.; Marcelis, A. T.; Zuilhof, H. Covalent surface modification of oxide surfaces. *Angewandte Chemie International Edition* **2014**, *53*, 6322–6356.

(54) Inal, S.; Rivnay, J.; Leleux, P.; Ferro, M.; Ramuz, M.; Brendel, J. C.; Schmidt, M. M.; Thelakkat, M.; Malliaras, G. G. A high transconductance accumulation mode electrochemical transistor. *Advanced Materials* **2014**, *26*, 7450–7455.

(55) Stavrinidou, E.; Leleux, P.; Rajaona, H.; Khodagholy, D.; Rivnay, J.; Lindau, M.; Sanaur, S.; Malliaras, G. G. Direct measurement of ion mobility in a conducting polymer. *Advanced Materials* **2013**, *25*, 4488–4493.

(56) Håkansson, A.; Han, S.; Wang, S.; Lu, J.; Braun, S.; Fahlman, M.; Berggren, M.; Crispin, X.; Fabiano, S. Effect of (3-glycidyloxypropyl) trimethoxysilane (GOPS) on the electrical properties of PEDOT: PSS films. *Journal of Polymer Science Part B: Polymer Physics* **2017**, *55*, 814–820.

(57) Elmahmoudy, M.; Inal, S.; Charrier, A.; Uguz, I.; Malliaras, G. G.; Sanaur, S. Tailoring the electrochemical and mechanical properties of PEDOT: PSS films for bioelectronics. *Macromolecular Materials and Engineering* **2017**, *302*, 1600497.

(58) Tan, E.; Pappa, A.-M.; Pitsalidis, C.; Nightingale, J.; Wood, S.; Castro, F. A.; Owens, R. M.; Kim, J.-S. A highly sensitive molecular structural probe applied to in situ biosensing of metabolites using PEDOT: PSS. *Biotechnology and Bioengineering* **2020**, *117*, 291–299.

(59) Lingstedt, L. V. Organic electrochemical transistor for biological applications. Ph.D. thesis, Johannes Gutenberg-Universität Mainz, 2019.

(60) D´ Angelo, P.; Tarabella, G.; Romeo, A.; Marasso, S. L.; Verna, A.; Cocuzza, M.; Peruzzi, C.; Vurro, D.; Iannotta, S. PEDOT: PSS morphostructure and ion-to-electron transduction and amplification mechanisms in organic electrochemical transistors. *Materials* **2018**, *12*, 9.

(61) Sezen, H.; Suzer, S. XPS for chemical-and charge-sensitive analyses. *Thin Solid Films* **2013**, *534*, 1–11.

(62) Skoog, D. A.; Holler, F. J.; Crouch, S. R. *Principles of instrumental analysis*; Cengage learning, 2017.

(63) Sezen, H. Photo-dynamic XPS for investigating photoinduced voltage changes in semiconducting materials. Ph.D. thesis, Bilkent Universitesi (Turkey), 2011.

(64) Habibullah, H. 30 Years of atomic force microscopy: Creep, hysteresis, cross-coupling, and vibration problems of piezoelectric tube scanners. *Measurement* **2020**, *159*, 107776.

(65) Binnig, G.; Quate, C. F.; Gerber, C. Atomic force microscope. *Physical review letters* **1986**, *56*, 930.

(66) Giessibl, F. J. Advances in atomic force microscopy. *Reviews of modern physics* **2003**, *75*, 949.

(67) Geisse, N. A. AFM and combined optical techniques. *Materials today* **2009**, *12*, 40–45.

(68) Guo, D.; Xie, G.; Luo, J. Mechanical properties of nanoparticles: basics and applications. *Journal of physics D: applied physics* **2013**, *47*, 013001.

(69) Özenler, S. Preparation of nanostructured interface by polymer grafting on various solid substrates for biosensor applications. **2021**,

(70) Sensi, M.; Berto, M.; Candini, A.; Liscio, A.; Cossarizza, A.; Beni, V.; Biscarini, F.;

Bortolotti, C. A. Modulating the faradic operation of all-printed organic electrochemical transistors by facile in situ modification of the gate electrode. *ACS Omega* **2019**, *4*, 5374–5381.

(71) Koutsouras, D. A.; Torricelli, F.; Gkoupidenis, P.; Blom, P. W. Efficient Gating of Organic Electrochemical Transistors with In-Plane Gate Electrodes. *Advanced Materials Technologies* **2021**, *6*, 2100732.

(72) Kergoat, L.; Piro, B.; Berggren, M.; Horowitz, G.; Pham, M.-C. Advances in organic transistor-based biosensors: from organic electrochemical transistors to electrolyte-gated organic field-effect transistors. *Analytical and bioanalytical chemistry* **2012**, *402*, 1813–1826.

(73) Desai, L. V.; Malik, H. A.; Sanford, M. S. Oxone as an inexpensive, safe, and environmentally benign oxidant for C- H bond oxygenation. *Organic letters* **2006**, *8*, 1141–1144.

(74) van der Pol, T. P.; Keene, S. T.; Saes, B. W.; Meskers, S. C.; Salleo, A.; van de Burgt, Y.; Janssen, R. A. The mechanism of dedoping PEDOT: PSS by aliphatic polyamines. *The Journal of Physical Chemistry C* **2019**, *123*, 24328–24337.

(75) Schmode, P.; Ohayon, D.; Reichstein, P. M.; Savva, A.; Inal, S.; Thelakkat, M. High-performance organic electrochemical transistors based on conjugated polyelectrolyte copolymers. *Chemistry of Materials* **2019**, *31*, 5286–5295.

(76) Tehrani, P.; Kanciurzewska, A.; Crispin, X.; Robinson, N. D.; Fahlman, M.; Berggren, M. The effect of pH on the electrochemical over-oxidation in PEDOT: PSS films. *Solid State Ionics* **2007**, *177*, 3521–3527.

(77) Tang, K.; Miao, W.; Guo, S. Crosslinked PEDOT: PSS Organic Electrochemical Transistors on Interdigitated Electrodes with Improved Stability. *ACS Applied Polymer Materials* **2021**, *3*, 1436–1444.

(78) Sangeeth, C. S.; Jaiswal, M.; Menon, R. Correlation of morphology and charge

transport in poly (3, 4-ethylenedioxythiophene)–polystyrenesulfonic acid (PEDOT–PSS) films. *Journal of Physics: Condensed Matter* **2009**, *21*, 072101.

(79) Beamson, G.; Briggs, D. High resolution XPS of organic polymers: the Scienta ESCA300 database, 1992. *Google Scholar There is no corresponding record for this reference*

(80) Brisk, M. A.; Baker, A. Shake-up satellites in X-ray photoelectron spectroscopy. *Journal of Electron Spectroscopy and Related Phenomena* **1975**, *7*, 197–213.

(81) Gardella, J. A.; Ferguson, S. A.; Chin, R. L. $\pi^* \leftarrow \pi$ shakeup satellites for the analysis of structure and bonding in aromatic polymers by X-ray photoelectron spectroscopy. *Applied spectroscopy* **1986**, *40*, 224–232.

(82) Pignataro, S.; Di Marino, R.; Distefano, G.; Mangini, A. Core ionization energies and multi-peak structure of esca bands in some pentatomic heterocyclic compounds. *Chemical Physics Letters* **1973**, *22*, 352–355.

(83) Chastain, J.; King Jr, R. C. Handbook of X-ray photoelectron spectroscopy. *Perkin-Elmer Corporation* **1992**, *40*, 221.

(84) Greczynski, G.; Kugler, T.; Keil, M.; Osikowicz, W.; Fahlman, M.; Salaneck, W. R. Photoelectron spectroscopy of thin films of PEDOT–PSS conjugated polymer blend: a mini-review and some new results. *Journal of Electron Spectroscopy and Related Phenomena* **2001**, *121*, 1–17.

(85) Li, S.; Kang, E.; Neoh, K.; Ma, Z.; Tan, K.; Huang, W. In situ XPS studies of thermally deposited potassium on poly (p-phenylene vinylene) and its ring-substituted derivatives. *Applied surface science* **2001**, *181*, 201–210.